Scheingross, J., Lamb, M. P. (2017): A Mechanistic Model of Waterfall Plunge Pool Erosion into Bedrock. - *Journal of Geophysical Research*, *122*, pp. 2079—2104.

DOI: http://doi.org/10.1002/2017JF004195

AGU PUBLICATIONS

JGR

Journal of Geophysical Research: Earth Surface

RESEARCH ARTICLE
10.1002/2017JF004195

**Key Points:**
- Plunge pool depth and radius are controlled by sediment tools and cover
- Vertical plunge pool incision outpaces lateral erosion and undercutting by 10-fold
- Knickzone retreat from drilling waterfalls can differ significantly from stream power models

**Supporting Information:**
- Supporting Information S1
- Datasets S1–S6

**Correspondence to:**
J. S. Scheingross,
jschein@gfz-potsdam.de

**Citation:**
Scheingross, J. S., & Lamb, M. P. (2017). A mechanistic model of waterfall plunge pool erosion into bedrock. *Journal of Geophysical Research: Earth Surface*, *122*, 2079–2104. https://doi.org/10.1002/2017JF004195

Received 3 JAN 2017
Accepted 15 SEP 2017
Accepted article online 24 SEP 2017
Published online 6 NOV 2017



# A Mechanistic Model of Waterfall Plunge Pool Erosion into Bedrock

**Joel S. Scheingross**[1,2] **and Michael P. Lamb**[1]

[1]Division of Geological and Planetary Sciences, California Institute of Technology, Pasadena, CA, USA, [2]Now at Helmholtz Centre Potsdam, German Research Center for Geosciences (GFZ), Potsdam, Germany

**Abstract** Landscapes often respond to changes in climate and tectonics through the formation and upstream propagation of knickzones composed of waterfalls. Little work has been done on the mechanics of waterfall erosion, and instead most landscape-scale models neglect waterfalls or use rules for river erosion, such as stream power, that may not be applicable to waterfalls. Here we develop a physically based model to predict waterfall plunge pool erosion into rock by abrasion from particle impacts and test the model against flume experiments. Both the model and experiments show that evolving plunge pools have initially high vertical erosion rates due to energetic particle impacts, and erosion slows and eventually ceases as pools deepen and deposition protects the pool floor from further erosion. Lateral erosion can continue after deposition on the pool floor, but it occurs at slow rates that become negligible as pools widen. Our work points to the importance of vertical drilling of successive plunge pools to drive upstream knickzone propagation in homogenous rock, rather than the classic mechanism of headwall undercutting. For a series of vertically drilling waterfalls, we find that upstream knickzone propagation is faster under higher combined water and sediment fluxes and for knickzones composed of many waterfalls that are closely spaced. Our model differs significantly from stream-power-based erosion rules in that steeper knickzones can retreat faster or more slowly depending on the number and spacing of waterfalls within a knickzone, which has implications for interpreting climatic and tectonic history through analysis of river longitudinal profiles.

## 1. Introduction

Bedrock waterfalls are ubiquitous in upland areas and can propagate upstream, or retreat, rapidly at rates up to, and in cases exceeding, $10^0$ to $10^3$ mm/yr (e.g., Anton et al., 2015; Gilbert, 1907; Hayakawa et al., 2008; Mackey et al., 2014), far outpacing typical fluvial vertical incision rates into bedrock (Portenga & Bierman, 2011). Waterfall retreat is often driven through erosion in bedrock-walled plunge pools at the base of waterfalls (e.g., Gilbert, 1890; Howard et al., 1994). As waterfalls retreat upstream, local base-level lowering causes adjacent hillslopes to steepen, resulting in increased erosion rates (Berlin & Anderson, 2009; DiBiase et al., 2015; Gallen et al., 2011; Mackey et al., 2014). In this way, plunge pool erosion can set the pace and style of landscape evolution. Despite numerous studies of the erosion and retreat of headcuts formed in sediment (e.g., Bennett et al., 2000; Flores-Cervantes et al., 2006; Stein et al., 1993), there exist few detailed studies of the mechanisms of waterfall erosion in rock (e.g., Bollaert & Schleiss, 2003; Haviv et al., 2010; Lamb & Dietrich, 2009; Young, 1985), and fundamental unknowns remain as to how waterfalls erode bedrock, retreat upstream, and respond to changes in forcing.

Here we focus on erosion in bedrock-walled waterfall plunge pools, which frequently occur at the base of waterfalls, regardless of rock type. For example, plunge pools are classically invoked (Gilbert, 1890) to promote waterfall retreat via undercutting a weak rock layer at a waterfall base to produce a cantilever caprock that eventually collapses under its own weight (Figure 1a). Retreat via headwall undercutting has been documented in flume experiments and select field examples with horizontally layered rock (Frankel et al., 2007; Gilbert, 1890; Holland & Pickup, 1976); however, many waterfalls in nature lack evidence for undercutting (e.g., Figure 1). Instead, upstream knickzone retreat through a series of waterfalls that primarily erode vertically, or *drill*, into their plunge pools has been proposed as an alternative mechanism in several landscapes (Howard et al., 1994; Lamb et al., 2007; Figure 1b). The ability of waterfalls to retreat upstream via headwall undercutting or vertical drilling should depend on the relative rates of vertical to lateral erosion in a plunge pool, as well as the rate of lowering of the downstream plunge pool lip. For example, vertical drilling may dominate if lateral erosion rates are small and if lowering of the downstream plunge pool lip allows

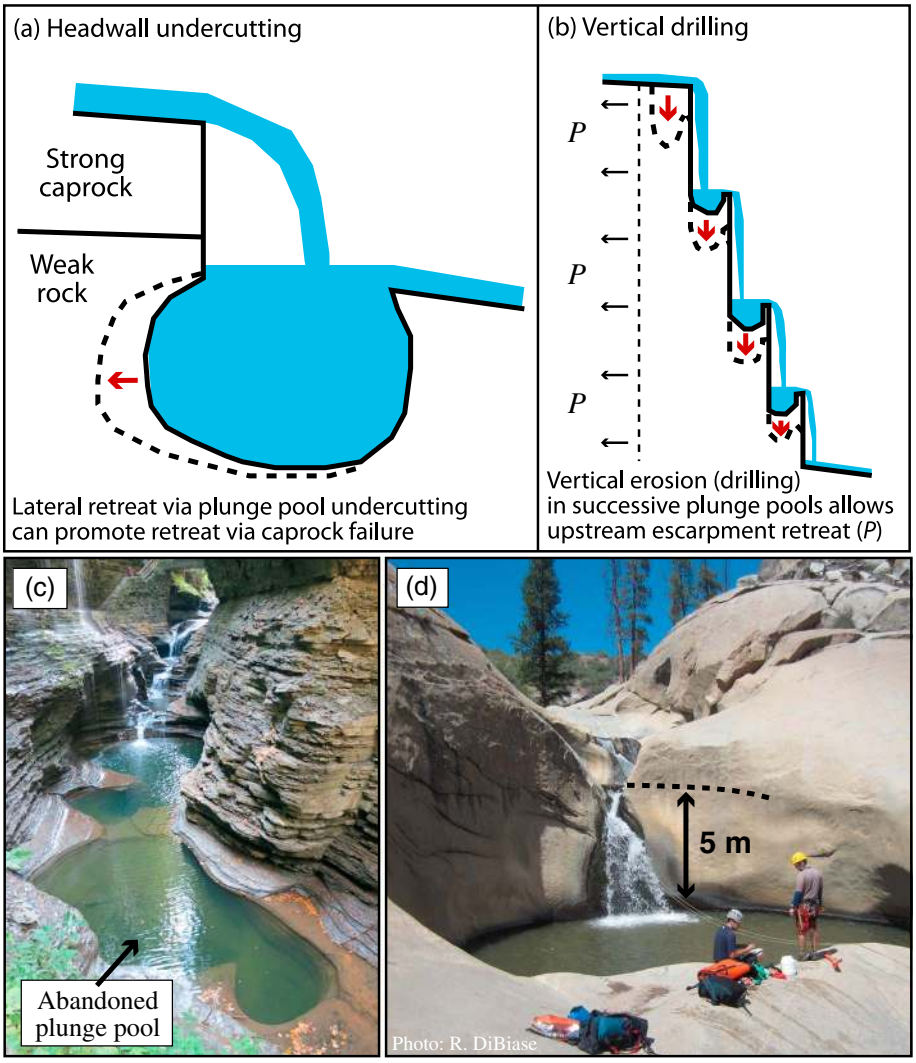


**Figure 1.** Schematic showing previously proposed waterfall retreat mechanisms for (a) headwall undercutting (Gilbert, 1890) and (b) vertical drilling of successive plunge pools (Howard et al., 1994; Lamb et al., 2007). (c) Waterfalls at Watkins Glen, NY, channel is ~8 m wide for scale, and (d) one of a series of waterfalls on Dry Meadow Creek, CA. Plunge pools in Figures 1c and 1d show no evidence of headwall undercutting.

sediment to be evacuated from the pool (Scheingross et al., 2017). Alternatively, sediment deposition on the pool floor or differences in rock strength between the pool floor and walls may promote high rates of lateral erosion relative to vertical incision, potentially leading to headwall undercutting as envisioned by Gilbert (1890) for Niagara Falls.

Currently, there exists no process-based model that can predict both vertical and lateral erosion of a bedrock plunge pool, thus limiting our ability to determine the conditions under which undercutting and drilling are applicable, as well as overall waterfall retreat rates. Instead, most landscape-scale models do not treat waterfalls and plunge pools explicitly and instead assume knickzone retreat follows fluvial erosion rules, such as stream power (Seidl et al., 1994; Stock & Montgomery, 1999) or saltation–abrasion (e.g., Chatanantavet & Parker, 2006; Crosby et al., 2007; Wobus et al., 2006). However, stream power models erroneously predict infinite erosion rates where bed slopes are vertical, which is common at waterfall faces. Saltation–abrasion models, on the other hand, predict no erosion at vertical waterfalls because particle hop lengths become infinitely long. Others have adapted stream power models to waterfalls by removing the slope dependency, assuming that waterfall retreat is proportional only to drainage area, that is,

$$P = kA^{\varphi}, \tag{1}$$

where $P$ is the upstream waterfall propagation rate, $A$ is the drainage area (which serves as a proxy for water discharge), and $k$ and $\phi$ are empirical constants that attempt to incorporate the effects of rock type, sediment supply, climate variability, waterfall geometry, and retreat mechanism (Brocard et al., 2016; Crosby & Whipple, 2006; Loget & Van Den Driessche, 2009; Rosenbloom & Anderson, 1994). A version of equation (1) that accounts for rock compressive strength and waterfall geometry exists (Hayakawa & Matsukura, 2003) but still requires an empirical constant to account for the influence of sediment supply, climate, and more.

Process-based models exist for failure of overhanging caprock developed by undercut plunge pools (e.g., Haviv et al., 2010; Hayakawa & Matsukura, 2010; Stein & LaTray, 2002); however, theory for pool erosion into rock that leads to undercutting has yet to be developed. Lamb et al. (2007) modified existing fluvial bedrock abrasion theory (Sklar & Dietrich, 2004) to predict abrasion of plunge pool bedrock floors via vertical impacts from particles that accelerate during free fall from the upstream waterfall brink and put this in a kinematic context to predict escarpment retreat from successive drilling plunge pools. The Lamb et al. (2007) model describes vertical erosion only, without a lateral erosion component. In addition, their model depends strongly on the plunge pool sediment transport capacity, $Q_{sc\_pool}$, which had not been investigated at the time of their study (Scheingross & Lamb, 2016).

Here we build on the Lamb et al. (2007) model for vertical pool incision and the Scheingross and Lamb (2016) model for sediment transport capacity of waterfall plunge pools to develop a theory for waterfall plunge pool vertical and lateral bedrock abrasion from impacting particles. We test the model against recent laboratory experiments that developed waterfall plunge pools from erosion of synthetic bedrock (Scheingross et al., 2017). Next, we use the model to examine the dominance of plunge pool undercutting versus vertical drilling for conditions common to natural landscapes. Finally, we use the model to explore what sets the rate of waterfall escarpment retreat via vertical drilling.

## 2. Theory

### 2.1. Conceptual Overview

Our model is designed to predict plunge pool bedrock erosion from abrasion by impacting particles and does not account for erosion via plucking (Bollaert & Schleiss, 2003; Lamb et al., 2015; Robinson et al., 2001), toppling (e.g., Baynes et al., 2015; Lamb & Dietrich, 2009; Lapotre et al., 2016; Weissel & Seidl, 1997), or other erosional processes such as bedrock weathering (e.g., Haviv et al., 2010). Observations of smooth and well-polished surfaces across a variety of waterfall plunge pools (e.g., Figure 1) suggest that abrasion is common and abrasion is often evoked or implied in studies of fluvial bedrock incision and waterfall plunge pool erosion (e.g., Gilbert, 1890; Lamb et al., 2007; Sklar & Dietrich, 2004).

We seek a model that can predict waterfall plunge pool erosion over timescales ranging from hours to millions of years in order to capture effects of individual floods as well as landscape response to changing climatic and tectonic forcing. Accurate erosion predictions require coupling hydrodynamics and sediment transport that drive erosion, but calculations must be simple enough to apply across large timescales during which landscapes evolve (e.g., Dietrich et al., 2003). To this end, we develop a plunge pool abrasion theory under the constraints of a channel-spanning, axisymmetric, bedrock-walled cylindrical plunge pool (Figure 2). Our theory is quasi two-dimensional in that plunge pools are allowed to erode vertically and laterally; however, we force pools to maintain cylindrical geometries with a free water surface where the waterfall jet impacts the plunge pool center. The assumed symmetry and free water surface may not be valid, for example, for waterfalls with headwalls that are strongly undercut. These geometric constraints allow for a semi-analytical solution; more complex pool shapes and waterfall jet geometries would likely require a computationally expensive 3-D simulation.

Conceptually, our model builds on previously proposed ideas (Howard et al., 1994; Lamb et al., 2007; Scheingross et al., 2017; Scheingross & Lamb, 2016) and works as follows: approaching a free overfall, water accelerates due to the loss of hydrostatic pressure at the brink (Hager, 1983; Rouse, 1936, 1937b). The water detaches from the face of a bedrock step, forming a sediment-laden waterfall that further accelerates during free fall (e.g., Stein et al., 1993). A plunge pool develops as the waterfall jet scours away sediment from the base and impacting particles abrade bedrock (e.g., Elston, 1918; Lamb et al., 2007 ; Sklar & Dietrich, 2004). Once a plunge pool develops, subsequent erosion is coupled to the topographic evolution of the pool

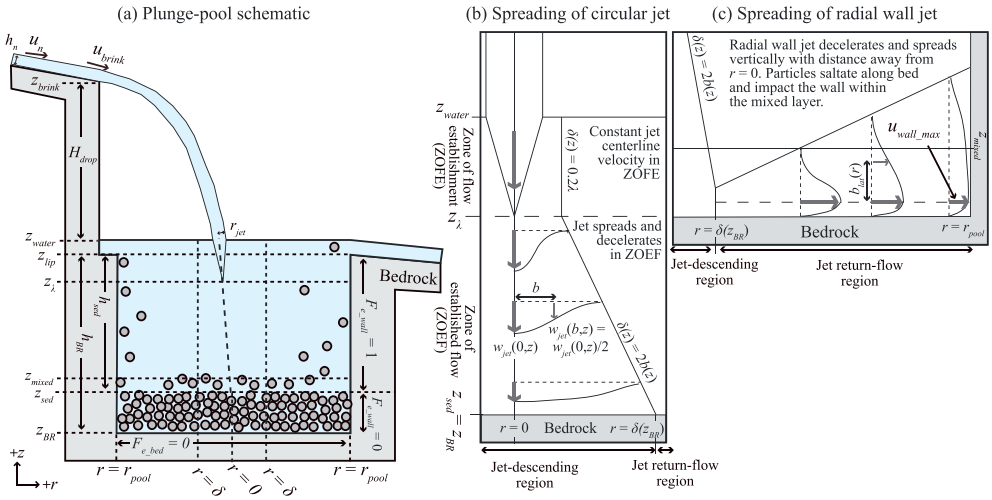


**Figure 2.** (a) Cartoon schematic of a plunge pool partially filled with sediment (modeled after Scheingross & Lamb, 2016) showing key variables. Additional schematics of spreading of the (b) circular and (c) radial jets, which impinge upon the plunge pool floor and walls, respectively. Variables used in plunge pool erosion theory are labeled: $b$ – half-width of descending waterfall jet, $b_{lat}$ – half-width of radial wall jet, $F_{e\_bed}$ – fraction of bedrock exposed on plunge pool floor, $F_{e\_wall}$ – fraction of bedrock exposed on plunge pool walls, $h_n$ – normal flow depth upstream of waterfall, $h_{BR}$ – plunge pool depth to bedrock, $h_{sed}$ – plunge pool depth to sediment, $H_{drop}$ – waterfall drop height, $r_{jet}$ – waterfall jet radius at impact with plunge pool water surface, $r_{pool}$ – plunge pool radius, $u_{brink}$ – water velocity at the waterfall brink, $u_n$ – normal flow velocity upstream of the waterfall, $u_{wall\_max}$ – maximum velocity of radial wall jet, $w_{jet}$ – vertical velocity of descending waterfall jet, $z_{BR}$ – elevation of plunge pool bedrock floor, $z_{brink}$ – elevation of the upstream waterfall brink, $z_{lip}$ – elevation of downstream plunge pool lip, $z_{mixed}$ – elevation of the top of the well-mixed layer near the pool floor, $z_{sed}$ – elevation of plunge pool alluvial floor, $z_{water}$ – elevation of plunge pool water surface, $z_\lambda$ – elevation of transition between ZOEF and ZOFE, $\delta$ – radius of jet-descending region, $\lambda$ – length of ZOFE, ZOFE – zone of flow establishment, ZOEF – zone of established flow.

(e.g., Alonso et al., 2002; Pagliara et al., 2006; Stein & Julien, 1993). As pools deepen, particle impact velocities slow due to drag from water within the pool, reducing bedrock erosion rates within the pool (Lamb et al., 2007). Furthermore, plunge pool sediment transport capacity decreases with increasing pool depth (Scheingross & Lamb, 2016), leading to the development of static sediment cover over the bedrock pool floor, inhibiting further vertical incision (Lamb et al., 2007; Scheingross et al., 2017; Sklar & Dietrich, 2001). Once alluviated, lateral erosion of the exposed pool sidewalls continues (Scheingross et al., 2017).

### 2.2. Modeling Framework

The model is developed using a cylindrical coordinate system where the vertical ($z$) and radial ($r$) coordinates are positive in the upward and outward directions, respectively, and $r = 0$ is along a vertical axis at the plunge pool center (Figure 2). We assume horizontal pool floors and vertical walls and treat vertical and lateral erosion as independent processes where erosion rates are averaged over the entire pool floor and walls, respectively, to maintain a cylindrical pool geometry. As pools can have fluctuating levels of sediment fill, the pool depth to sediment, $h_{sed} = z_{lip} - z_{sed}$, is distinguished from the depth to bedrock, $h_{BR} = z_{lip} - z_{BR}$, where $z_{lip}$, $z_{sed}$, and $z_{BR}$ are the elevations of the downstream plunge pool bedrock lip, the sediment fill, and the bedrock floor, respectively (Figure 2). If there is no sediment deposited within the pool, $h_{sed} = h_{BR}$ and $z_{sed} = z_{BR}$. Following Scheingross and Lamb (2016), no predictions are made when pools aggrade to within ~7 grain diameters of $z_{lip}$, based on experimental observations of fluidized sediment beds for these conditions.

Following previous abrasion theory (Lamb et al., 2007; Sklar & Dietrich, 2004), the volumetric erosion rate per unit bed area ($E$) can be parameterized as the product of the volume of rock detached per particle impact ($V_i$), the rate of particle impacts per unit bed area per time ($I_r$), and the fraction of exposed bedrock ($F_e$), such that,

$$E = V_i I_r F_e. \tag{2}$$

Lamb et al. (2008) modified equation (2) for mixed suspended and bed load transport using a near-bed volumetric sediment concentration ($c_o$) and particle impact velocity ($w_i$), such that,

$$E = \kappa A_1 c_o w_i^3 F_e. \tag{3}$$

In equation (3), $\kappa$ is a dimensional constant [$T^2/L^2$] that accounts for bedrock material properties (Sklar & Dietrich, 2004);

$$\kappa = \frac{\rho_s k_Y}{\sigma_T^2}, \tag{4}$$

where $\rho_s$ and $\sigma_T$ are rock density and tensile strength, respectively, $k_Y \sim 0.05$ MPa is an empirical constant related to the energy required to erode a unit volume of rock and rock elasticity (Lamb et al., 2015), and $A_1 < 1$ is a constant that we set equal to 0.5 reflecting that grains can be advected both toward and away from the bedrock surface. Equation (3) can be applied across different field sites and laboratory experiments because $\rho_s$ and $\sigma_T$ account for different rock types and the constant $k_y$ does not vary strongly (Sklar & Dietrich, 2004).

We modify equation (3) to predict spatially variable plunge pool vertical and lateral abrasion rates, $E_{vert}(r)$ and $E_{lat}(z)$, respectively. We replace $c_o$ with the spatially variable sediment concentration along the plunge pool floor and walls, $c_{bed}(r)$ and $c_{wall}(z)$, and separately parameterize vertical and lateral particle- mpact velocities, $w_{vert}(r)$ and $u_{lat}(z)$, as well as the fraction of exposed bedrock on the plunge pool floor and walls, $F_{e\_bed}(r)$ and $F_{e\_wall}(z)$. Our equations for plunge pool abrasion on the pool floor and walls are thus

$$E_{vert}(r) = \kappa A_1 c_{bed}(r) w_{vert}^3(r) F_{e\_bed}(r), \tag{5a}$$

$$E_{lat}(z) = \kappa A_1 c_{wall}(z) u_{lat}^3(z) F_{e\_wall}(z). \tag{5b}$$

To define representative erosion rates that can be applied across the entire plunge pool floor and walls, we use the radially averaged vertical erosion rate ($\overline{E_{vert}}$) and depth-averaged lateral erosion rate ($\overline{E_{lat}}$):

$$\overline{E_{vert}} = \frac{2\pi}{A_{pool}} \int_{r=0}^{r=r_{pool}} E_{vert}(r) r dr, \tag{6a}$$

$$\overline{E_{lat}} = \frac{1}{h_{BR}} \int_{z=z_{bp}}^{z=z_{BR}} E_{lat}(z) dz, \tag{6b}$$

in which $r_{pool}$ is the plunge pool radius and $A_{pool}$ is the cross-sectional area of the pool floor. In the following two subsections, we derive the vertical and lateral abrasion theories, specifying controls on the sediment concentration, particle impact velocity, and fraction of exposed bedrock in equations (5a) and (5b).

### 2.3. Plunge Pool Vertical Abrasion

#### 2.3.1. Sediment Concentration Along the Bed

To predict the near-bed sediment concentration of a plunge pool for a given sediment supply, we use the model of Scheingross and Lamb (2016) summarized here. Similar to the model framework discussed above, the Scheingross and Lamb (2016) theory predicts plunge pool hydraulics and sediment transport assuming steady, axisymmetric flow within the plunge pool. As a waterfall jet impinges into a standing pool of water, it travels a finite distance, $\lambda$, over which the jet maintains a constant centerline velocity (Figure 2). This distance is empirically found as $\lambda = 13.52 r_{jet} \sin\beta$, where $r_{jet}$ is the waterfall jet radius and $\beta$ is the jet impact angle with respect to the pool water surface (Beltaos, 1976; Beltaos & Rajaratnam, 1973; Stein et al., 1993), and it defines a region referred to as the zone of flow establishment (ZOFE; e.g., Albertson et al., 1950; Rajaratnam, 1976). Beyond the ZOFE (i.e., at $[z_{water} - z] > \lambda$, where $z_{water}$ is the elevation of the plunge pool water surface), the jet enters the zone of established flow (ZOEF) where friction from the surrounding water causes deceleration at the jet centerline as the jet spreads and mixes with the surrounding fluid (e.g., Abramovich & Schindel, 1963; Giger et al., 1991).

Scheingross and Lamb (2016) define the region where the jet is primarily descending toward the plunge pool floor as the "jet-descending region," and the annulus outside of the jet-descending region as the "jet return-flow region" (Figure 2). The boundary between these regions is defined at $r = 2b(z) = \delta(z)$ (Figure 2), where $b(z)$

is the distance at which the jet decreases to half its centerline velocity and can be approximated as (e.g., Abramovich & Schindel, 1963; Giger et al., 1991)

$$b(z) = \begin{cases} 0.1\lambda, & \text{for } z_\lambda < z < z_{\text{water}}, \\ 0.1(z_{\text{water}} - z), & \text{for } z_{\text{sed}} < z < z_\lambda. \end{cases} \tag{7}$$

Sediment mobilized by the impinging jet is assumed to be entrained into a thin, well-mixed layer with constant sediment concentration (extending to an elevation of $z_{\text{mixed}}$ calculated following Scheingross & Lamb, 2016; Figure 2) and above which sediment concentration decays, similar to standard theory for turbulent, unidirectional flows (e.g., McLean, 1992; Rouse, 1937a). In the radial direction, sediment concentration is assumed to be constant within the jet-descending region but decays nonlinearly with increasing radial distance in the return flow region. Following previous theory for suspended sediment transport (Rouse, 1937a), Scheingross and Lamb (2016) balance upward and lateral sediment transport due to turbulent mixing and particle settling in the return-flow region. Sediment mixing scales with a diffusive length scale, $L_d$, which represents a balance between turbulence (parameterized through a kinematic eddy viscosity) and net particle setting velocity that accounts for gravitational settling against the upward return flow. The resulting distribution of sediment concentration within the pool, $c(r, z)$, is

$$c(r,z) = c_b \exp\left(-\frac{(z - z_{\text{mixed}})}{L_d}\right)\left(\frac{I_0(r/L_d) + \frac{I_1(r_{\text{pool}}/L_d)}{K_1(r_{\text{pool}}/L_d)}K_o(r/L_d)}{I_0(\delta/L_d) + \frac{I_1(r_{\text{pool}}/L_d)}{K_1(r_{\text{pool}}/L_d)}K_0(\delta/L_d)}\right), \tag{8}$$

where $c_b$ is the sediment concentration within the near-bed well-mixed layer in the jet-descending region. $I_0$, $K_0$, $I_1$, and $K_1$ are the modified Bessel functions of the first and second kind of orders 0 and 1, respectively, which occur in the solution due to the cylindrical geometry imposed. At the bedrock pool floor and when $z < z_{\text{mixed}}$, the exponential term reduces to unity such that

$$c_{\text{bed}}(r) = c_b\left(\frac{I_0(r/L_d) + \frac{I_1(r_{\text{pool}}/L_d)}{K_1(r_{\text{pool}}/L_d)}K_o(r/L_d)}{I_0(\delta/L_d) + \frac{I_1(r_{\text{pool}}/L_d)}{K_1(r_{\text{pool}}/L_d)}K_0(\delta/L_d)}\right). \tag{9}$$

Equation (9) allows calculation of $c_{\text{bed}}(r)$, which is needed to drive the erosion model (equations (5a) and (5b)). However, solving equation (9) for supply-limited conditions requires calculation of $c_b$, for which an additional constraint given by the sediment supply to the pool is needed. For plunge pools that experience erosion of the bedrock floor, we assume that sediment flux out of the pool is equal to the sediment supply to the pool from upstream. Thus, sediment does not accumulate in the pool (or else sediment cover would prevent bedrock erosion), and the erosion rate is assumed to be slow enough such that sediment produced within the pool is negligible compared to the supply from upstream. These conditions should hold when the sediment supply is less than the transport capacity of the plunge pool. Thus, under steady-state sediment flux through the pool, mass balance dictates that

$$Q_s = \frac{c_b Q_w}{(z_{\text{water}} - z_{\text{lip}})}\chi, \tag{10}$$

where $Q_s$ and $Q_w$ are the sediment supply and water discharge, respectively, and $\chi$ is the integral of normalized sediment concentration where water spills out of the pool downstream, that is,

$$\chi = \int_{z_{\text{lip}}}^{z_{\text{water}}} \frac{c(r_{\text{pool}}, z)}{c_b} dz, \tag{11}$$

in which $c(r_{\text{pool}}, z)$ is the vertical concentration profile along the pool wall found from equation (8). Rearranging equation (10), we can solve for $c_b$,

$$c_b = \frac{Q_s}{Q_w}\frac{(z_{\text{water}} - z_{\text{lip}})}{\chi}, \tag{12}$$

and therefore $c_{\text{bed}}(r)$ using equation (9). When sediment supply exceeds transport capacity, the plunge pool bedrock floor is alluviated, there is no vertical erosion, and $c_b$ can be calculated for transport-limited conditions following Scheingross and Lamb (2016).

#### 2.3.2. Vertical Particle Impacts

We assume particles impact the bedrock pool floor because of grains that are re-entrained by the jet within the pool and from grains that fall from the waterfall brink upstream. The grains falling from the waterfall brink are assumed to be limited to the jet-descending region where the waterfall jet impacts the pool floor ($r < \delta$). For cases when plunge pools have radii smaller than the jet-descending region, impacts from grains falling from the waterfall brink should act to rapidly widen plunge pools via sidewall impacts during their descent (Scheingross et al., 2017). Therefore, we assume that plunge pools must maintain a minimum radius, $r_{min}$, that grows at the same rate as the expansion of the jet-descending region in the ZOEF, that is,

$$r_{min} = 0.2(z_{water} - z_{BR}), \tag{13}$$

such that $r_{min} = \delta(z_{BR})$ for $z_{BR} < z_\lambda$.

Using nonlinear averaging to account for the cubic dependence of erosion on impact velocity (equations (5a) and (5b)), the effective vertical impact velocity at the pool floor is

$$w_{vert}(r) = \begin{cases} \left( w_{vert\_wf}^3 \frac{c_{wf}}{c_b} + w_{vert\_susp}^3 \left[ 1 - \frac{c_{wf}}{c_b} \right] \right)^{1/3} & \text{for } r < \delta, \\ w_{vert\_susp}, & \text{for } r > \delta, \end{cases} \tag{14}$$

in which $w_{vert\_wf}$ and $w_{vert\_susp}$ are impacts from grains falling from the waterfall brink and grains re-entrained within the pool, respectively. $c_{wf}$ is the near-bed volumetric concentration of grains within the jet-descending region ($r < \delta$) that fall from the top of the waterfall (Figure 2) and is found from mass balance:

$$c_{wf} = \frac{Q_s}{w_{vert\_wf} A_{jdr}}, \tag{15}$$

where $A_{jdr} = \pi\delta^2$ is the area of the bed within the jet-descending region (if $r_{pool} < \delta$, then $\delta = r_{pool}$). Equation (15) assumes that grains falling from the waterfall brink are well mixed within the jet-descending region (Figure 2) and are not deflected within the impingement zone where the vertically descending jet turns along the pool floor as a radial wall jet. The latter assumption should hold so long as $h_{BR}$ is large compared to the thickness of radial wall jets within the jet-descending region, which is often the case for natural plunge pools (Scheingross & Lamb, 2016; Table S1 in the supporting information).

We assume $w_{vert\_susp}$ in equation (14) is set by the net particle settling velocity, $w_{net}$, as defined by Scheingross and Lamb (2016):

$$w_{vert\_susp} = w_{net} = w_s - w_{up}, \tag{16}$$

which represents a balance between gravitational particle settling, $w_s$, and upward-directed return flow, $w_{up}$.

The impact velocity for grains falling from the waterfall, $w_{vert\_wf}$, is calculated by conservation of momentum in the vertical dimension considering the force of gravity, $F_g$, which accelerates particles to the bed, and drag, $F_{d\_jet}$, which can accelerate or decelerate particles depending on the relative velocities of the particle and waterfall jet, as

$$\rho_s V_p \frac{dw_{particle}(z)}{dt} = F_g - F_{d\_jet}, \tag{17}$$

where $w_{particle}(z)$ and $V_p$ are the particle velocity and particle volume, respectively. Using the definition $w_{particle}(z) = dz/dt$, equation (17) can be rewritten to describe changes in particle velocity as a function of fall distance rather than time as

$$\rho_s V_p w_{particle} \frac{dw_{particle}(z)}{dz} = F_g - F_{d\_jet}. \tag{18}$$

The forces are defined as

$$F_g = (\rho_s - \rho_f) V_p g, \tag{19}$$

$$F_{d\_jet} = \frac{1}{2} \rho_f A_p C_{drag} \, \mathrm{sgn}\left( \overline{w_{jet}(z)} - w_{particle}(z) \right) \left( \overline{w_{jet}(z)} - w_{particle}(z) \right)^2, \tag{20}$$

where sgn is the sign function, $\overline{w_{jet}(z)}$ is the radially averaged waterfall jet velocity, $\rho_f$ is the fluid density, $g$ is gravitational acceleration, $A_p$ is the particle cross-sectional area, and $C_{drag}$ is a drag coefficient found using

Ferguson and Church (2004). We assume that particles fall within an aerated waterfall jet (both from the waterfall brink to the plunge pool water surface and within the plunge pool itself) and set the fluid density to $\rho_f = 0.7\rho_w$, where $\rho_w$ is the density of water, to reflect the fact that waterfall jets typically have air concentrations varying between ~0.1 and 0.6 (Valle & Pasternack, 2006).

Combining equations (18)–(20) results in a first-order nonlinear differential equation, which, to calculate $w_{vert\_wf}$, must be solved in three separate domains: $z_{brink}$ to $z_{water}$, $z_{water}$ to $z_\lambda$, and $z_\lambda$ to $z_{sed}$, where $z_{brink}$ and $z_\lambda$ are the elevations of the upstream waterfall brink and the transition between the ZOFE and ZOEF in the plunge pool, respectively (Figure 2). In the first domain, from the waterfall brink to the plunge pool water surface, we calculate the waterfall jet velocity along the jet centerline, $w_{jet}(z)$, assuming conservation of energy (e.g., Scheingross & Lamb, 2016; Stein et al., 1993) and neglect energy losses from air drag or wind such that

$$w_{jet}(z) = \sqrt{u_{brink}^2 + 2g(z_{brink} - z)}, \text{for } z > z_{water}, \tag{21}$$

where $u_{brink}$ is the horizontal water velocity at the upstream waterfall brink (Figure 2). In the second and third domains, which corresponds to the ZOFE and ZOEF, respectively, established turbulent jet theory (e.g., Albertson et al., 1950; Stein et al., 1993) shows that the jet centerline maintains a constant velocity in the ZOFE and decelerates with distance in the ZOEF, such that,

$$w_{jet}(r=0,z) = \begin{cases} w_{jet}(0, z_{water}), & \text{for } z_\lambda < z < z_{water}, \\ w_{jet}(0, z_{water})\sqrt{\dfrac{\lambda}{z_{water} - z}}, & \text{for } z < z_\lambda. \end{cases} \tag{22}$$

Moving away from the jet centerline, velocity profiles are self-similar and velocity decays with radial distance (e.g., Abramovich & Schindel, 1963; Albertson et al., 1950). We calculate the radially averaged jet velocity in both the ZOEF and the ZOFE by integrating over an established formulation for circular jets (Beltaos & Rajaratnam, 1974) as

$$\overline{w_{jet}(z)} = \frac{2\pi}{A_{jdr}} \int_{r=0}^{r=\delta} w_{jet}(0,z) \exp\left[-0.69(r/b(z))^2\right] r dr, \text{for } z < z_{water}. \tag{23}$$

Finally, we solve for the final particle impact velocity numerically using an explicit finite difference scheme by combining equations (18)–(23) to solve for the particle impact velocity at the water surface, the transition between the ZOFE and ZOEF, and the plunge pool floor.

Vertical particle impacts only produce erosion for cases when grains have sufficient inertia to overcome the effect of viscous dampening (e.g., Joseph et al., 2001; Schmeeckle et al., 2001), which is accounted for by setting $w_{vert}(r) = 0$ below a critical particle Stokes number, St, of 75 (Lamb et al., 2008; Scheingross et al., 2014).

#### 2.3.3. Fraction of Bed Exposed

Following the framework of Sklar and Dietrich (2004), we calculate the fraction of bedrock exposed on the plunge pool floor assuming that patchy sediment deposition across the floor creates a static cover that scales linearly with the ratio of the near-bed sediment concentration to the sediment concentration at capacity, $c_{bed\_capacity}(r)$, that is,

$$F_{e\_bed}(r) = 1 - \frac{c_{bed}(r)}{c_{bed\_capacity}(r)}, \text{for } c_{bed}(r) < c_{bed\_capacity}(r), \tag{24a}$$

$$F_{e\_bed}(r) = 0, \text{for } c_{bed}(r) > c_{bed\_capacity}(r), \tag{24b}$$

where $c_{bed\_capacity}(r)$ is calculated following Scheingross and Lamb (2016; their equation (26)). Substituting equations (9), (14), and (24) into equation (5a) allows for calculation of plunge pool vertical erosion rate.

### 2.4. Plunge Pool Lateral Abrasion

#### 2.4.1. Sediment Concentration Along the Walls

Similar to sediment concentration at the pool floor, we employ the Scheingross and Lamb (2016) theory to calculate spatially variable sediment concentration along the plunge pool walls:

$$c_{wall}(z) = c_{bed}(r_{pool}) \exp\left(-\frac{(z - z_{mixed})}{L_d}\right), \tag{25}$$

where $c_{bed}(r_{pool})$ is found by combining equations (9) and (12) for cases when the pool bedrock floor is exposed. For $z_{sed} < z < z_{mixed}$, there is no vertical variation in sediment concentration and equation (25) reduces to $c_{wall}(z) = c_{bed}(r_{pool})$.

When sediment supply exceeds the predicted plunge pool sediment transport capacity, pool floors become alluviated with a static sediment cover, but lateral erosion can still occur on exposed pool walls (Scheingross et al., 2017). For these cases, we use the Scheingross and Lamb (2016) theory to first set $z_{sed}$ to the predicted equilibrium pool depth and then calculate $c_{wall}(z)$ at capacity by combining equations (9) and (25) while setting $c_b$ to its value at capacity following Scheingross and Lamb (2016; their equation (30)) and use this value of sediment concentration to drive lateral erosion predictions.

#### 2.4.2. Lateral Particle Impacts

Lateral impacts are assumed to occur as near-bed particles become entrained within the radial wall jet along the pool floor and are advected into the pool sidewalls. For lateral impacts to occur, grains must have sufficient inertia to detach from the fluid and maintain lateral trajectories toward the wall at the point where the fluid is redirected vertically by the confining walls (Figure 2). In Appendix A, we compare characteristic length scales over which particles slow in the absence of a jet relative to a jet-turning length scale and show that this is a reasonable assumption near the bed, but is likely violated higher on the pool walls. As such, all lateral impacts are assumed to be concentrated between $z_{sed} < z < z_{mixed}$ where the radial wall jet advects particles toward the wall and that impacts do not occur for $z > z_{mixed}$ where particles are primarily advected vertically.

We assume grains within the mixed layer saltate along the bed and therefore impact the pool wall at a characteristic saltation velocity, $u_s$. Recent compilation of experimental data for shear flow in rivers (Chatanantavet et al., 2013) suggests $u_s$ scales with the depth-averaged flow velocity, $U$, that is,

$$u_s = 0.6U. \tag{26}$$

Equation (26) is assumed to hold for plunge pools, but we replace $U$ with the local velocity of the radial wall jet at the point of impingement on the pool wall, $u_{wall}(r_{pool}, z)$, and use a nonlinear average to account for the fact that erosion scales with the cube of impact velocity (equation (3)).

Similar to vertically descending jets, radial wall jets display self-similar velocity structures that closely match those of planar wall jets (Launder & Rodi, 1983). We describe variation in radial velocity along the plunge pool wall using a planar wall jet relation (Rajaratnam, 1976; Verhoff, 1963), which has been previously applied to radial wall jets (e.g., Ghaneeizad et al., 2015):

$$u_{wall}\left(r_{pool}, z\right) = 1.48u_{wall\_max}\left(\frac{z}{b_{lat}\left(r_{pool}\right)}\right)^{1/7}\left[1 - \text{erf}\left(0.68\frac{z}{b_{lat}\left(r_{pool}\right)}\right)\right], \tag{27}$$

where erf is the error function and $u_{wall\_max}$ is the maximum fluid lateral velocity at the plunge pool wall. For radial wall jets, $u_{wall\_max}$ can be calculated as (e.g., Ghaneeizad et al., 2015; Rajaratnam, 1976)

$$u_{wall\_max} = 2.06w_{jet}(0, z_{water})\frac{r_{jet}}{r_{pool}}, \tag{28}$$

where $r_{jet}$ is the radius of the impinging waterfall jet at $z = z_{water}$ calculated following Scheingross and Lamb (2016). Application of equation (27) requires specifying the radial jet half width at the pool wall, $b_{lat}(r_{pool})$ (i.e., the vertical distance from the jet centerline at which jet velocity drops to half its maximum value; Figure 2), which we approximate with an empirical relation for radial wall jets (Rajaratnam, 1976):

$$b_{lat}(r) = 0.09r. \tag{29}$$

Particle lateral impact velocities are calculated assuming $u_{lat} = u_s$, combining equations (26)–(29) and performing nonlinear averaging over the mixed layer:

$$u_{lat} = 0.6\left(\frac{\int_{z_{sed}}^{z_{mixed}} u_{wall}^3\left(r_{pool}, z\right)dz}{\left(z_{mixed} - z_{sed}\right)}\right)^{(1/3)}, \text{for } z < z_{mixed}. \tag{30}$$

Following the assumption of no impacts above the mixed layer, we set $u_{lat} = 0$ for $z > z_{mixed}$. Finally, lateral impacts that fall below the threshold for viscous dampening (St < 75) are neglected.

#### 2.4.3. Fraction of Pool Walls Exposed

Vertical plunge pool walls do not experience partial cover. As such, we use a binary function to estimate the $F_{e\_wall}$, that is,

$$F_{e\_wall}(z) = \begin{cases} 1, & \text{for } z > z_{sed}, \\ 0, & \text{for } z < z_{sed}. \end{cases} \tag{31}$$

Finally, inserting equations (25), (30), and (31) into (5b) allows for the calculation of plunge pool lateral erosion.

### 2.5. Waterfall Escarpment Retreat

For cases when plunge pool vertical incision greatly outpaces lateral erosion, waterfall retreat should be dominated by drilling of successive plunge pools (Howard et al., 1994; Scheingross et al., 2017). The plunge pool erosion model developed in sections 2.1–2.4 can be used within the Lamb et al. (2007) kinematic framework to predict the upstream propagation rate of a knickzone made up of a series of waterfall plunge pools. Assuming that knickzones have a stair-stepped shape composed only of vertical waterfalls and their associated plunge pools (Figure 1b), conservation of mass dictates that the upstream propagation rate is (Lamb et al., 2007)

$$P = \frac{mE_{vert}2r_{pool}}{H_{kz}}, \tag{32}$$

where $m$ is the number of drilling waterfall plunge pools within the knickzone and $H_{kz}$ is the total knickzone relief. Application of equation (32) requires specification of $m$, $r_{pool}$, and $H_{kz}$ (e.g., from a reference site) and assumes that the creation of new waterfall plunge pools at the top of the escarpment is not a rate-limiting process.

### 2.6. Model Application

Our model predicts that vertical and lateral plunge pool erosion rates are controlled by nine key variables: water discharge, sediment supply, median grain size, reach-averaged channel width and flow-depth, plunge pool depth and radius, waterfall drop height, and bedrock tensile strength. In contrast, previous models such as equation (1) have fewer explicit dependencies and instead attempt to incorporate these variables through coefficients and exponents that are not known a priori and must be locally calibrated. While our theory also makes use of several empirically derived constants to describe turbulent jet hydrodynamics (e.g., equations (7), (23), and (27)), sediment transport (e.g., equation (26)), and bedrock erosion (e.g., equation (3)), in all cases we use commonly accepted values for these constants that are often based on carefully scaled laboratory experiments. Therefore, the theory should be applicable to landscapes that differ in rock type, climatic regime, and sediment supply, as well as across both field and laboratory scales.

We evaluate the plunge pool erosion model by comparing model predictions to previous experimental observations (Scheingross et al., 2017). We additionally compare measurements of vertical erosion to predictions from the Lamb et al. (2007) plunge pool erosion model where we use the theory of Scheingross and Lamb (2016) to solve for plunge pool sediment transport capacity. Full experimental details are described in Scheingross et al. (2017); in brief, these experiments investigated the formation and evolution of waterfall plunge pools formed by sediment impacts into an initially planar surface using polyurethane foam as bedrock simulant (Lamb et al., 2015; Scheingross et al., 2014). Two experiments were performed varying grain size and sediment supply. The first experiment ('Exp1') used 2.4 mm diameter sediment fed at constant water discharge and sediment supply. In Exp1, the pool deepened until sediment supply exceeded the transport capacity, after which the pool partially filled with sediment, halting vertical erosion, while lateral erosion of the pool walls continued at low rates. The second experiment ('Exp2') used coarser, 7 mm diameter sediment with conditions identical to Exp1 for the first 14.8 h, during which the pool eroded vertically without depositing sediment. For the final 36.2 h of Exp2, sediment supply was increased by a factor of 5, forcing aggradation of the pool floor while lateral erosion continued. The range in plunge pool depth and radii achieved in the experiments results in approximately order of magnitude variation in the nondimensional variables that are thought to govern plunge pool sediment transport and are within the range observed in field surveys (Scheingross et al., 2017; Scheingross & Lamb, 2016), such that the dynamics observed in the laboratory

should scale to field cases. To compare the theory to the experiments, we use the boundary conditions from the experiments (Table S2) and set an initial pool geometry of $r_{pool} = h_{BR} = 1$ cm.

We also explore model predictions at field scale using a series of waterfalls in Fox Creek, San Gabriel Mountains, California, as a reference site, where waterfalls are interpreted to be retreating upstream following base-level fall (DiBiase et al., 2015). The reference site approach allows exploring model sensitivity to a single variable while holding other parameters constant at physically reasonable values. For the Fox Creek site, we input a 2 year recurrence interval discharge ($Q_w = 7.3$ m$^3$/s) and use average values for plunge pool radius, waterfall drop height, grain size, and upstream channel width as surveyed by Scheingross and Lamb (2016; Table S1). Because plunge pools were partially filled with sediment during surveying, we set $h_{BR} = 2$ m (the maximum value reported by Scheingross & Lamb, 2016). Finally, we estimate a reference sediment supply of $Q_s = 1.2 \times 10^{-2}$ m$^3$/s based on the 22.8 km$^2$ drainage area at the falls, assuming an intermittency factor of 0.01 and applying a 0.165 mm/yr basin-averaged erosion rate (DiBiase et al., 2015). While variability in both water discharge and sediment supply influence the rate and style of erosion (e.g., DiBiase & Whipple, 2011; Lague et al., 2005), we use constant reference values to explore the model response to simple scenarios of a change in forcing. Plunge pool erosion predictions require estimates of the river hydraulics upstream of the waterfall, which we calculate assuming steady, uniform flow ($\tau_b = \rho_f g h_n S$, where $\tau_b$ is the bed shear stress and $h_n$ and $S$ are normal flow depth and average channel slope upstream of the waterfall, respectively) and conservation of mass ($Q_w = u_n W h_n$, where $u_n$ and $W$ are the normal river flow velocity and reach-averaged channel width, respectively). We apply an established empirical fit to estimate the river friction factor ($C_{f\_river} = [8.1(h_n/[3D])^{1/6}]^{-2}$ (Garcia, 2008), where $D$ is the representative grain diameter).

Finally, we assess how waterfall erosion processes may change knickzone retreat and landscape evolution predictions by comparing escarpment retreat predictions made with our model against those from existing, low-gradient bedrock erosion theory, which is often used to model knickzone retreat (e.g., Bishop et al., 2005; Crosby et al., 2007; Seidl et al., 1994). Again using Fox Creek as an example, we predict escarpment retreat with equation (32), where we set $H_{kz} = 83$ m based on the sum of the drop heights of the eight active waterfalls within the knickzone (Table S1). We assume the knickzone is made up only of vertical waterfalls and their associated plunge pools, so that the total knickzone length is $2mr_{pool} = 42$ m, giving an averaged knickzone slope, $S_{kz}$, of 63°. We compare predictions with the saltation–abrasion model (Sklar & Dietrich, 2004), the total load model (Lamb et al., 2008), and a shear stress model where vertical fluvial erosion rate, $E_{river}$, scales with bed shear stress (e.g., Howard & Kerby, 1983), that is,

$$E_{river} = K\tau_b^a, \tag{33}$$

where $K$ is an empirical constant calibrated such that $E_{river} = 0.165$ mm for representative conditions at Fox Creek. We set $a = 1.5$ such that equation (33) follows the same scaling as unit stream power (Whipple & Tucker, 1999). Equation (33) is similar to celerity models (equation (1)) that are commonly used to model knickzone retreat, but equation (33) allows examination of the influence of changes in channel slope on erosion rate. We drive low-gradient fluvial incision models using a channel slope equivalent to the reach-averaged slope across the knickzone ($S_{kz} = 63°$ for Fox Creek), and because fluvial incision models predict vertical erosion rates, we divide $E_{river}$ by $S_{kz}$ to predict a horizontal escarpment retreat rate for comparison with equation (32), that is,

$$P = E_{river}/S_{kz}. \tag{34}$$

We also compare our predictions to equation (1) by taking advantage of the fact that discharge and drainage area tend to scale linearly in the San Gabriel Mountains (DiBiase & Whipple, 2011), such the equation (1) can be rewritten as

$$P \propto Q_w^{\varphi}, \tag{35}$$

and $\phi$ is left as a free parameter.

## 3. Results

### 3.1. Comparison With Experimental Data

The theory predicts the same bulk behavior as observed in the experiments with developing pools and a fixed downstream pool lip (Scheingross & Lamb, 2016). Pools first deepen and widen resulting in a

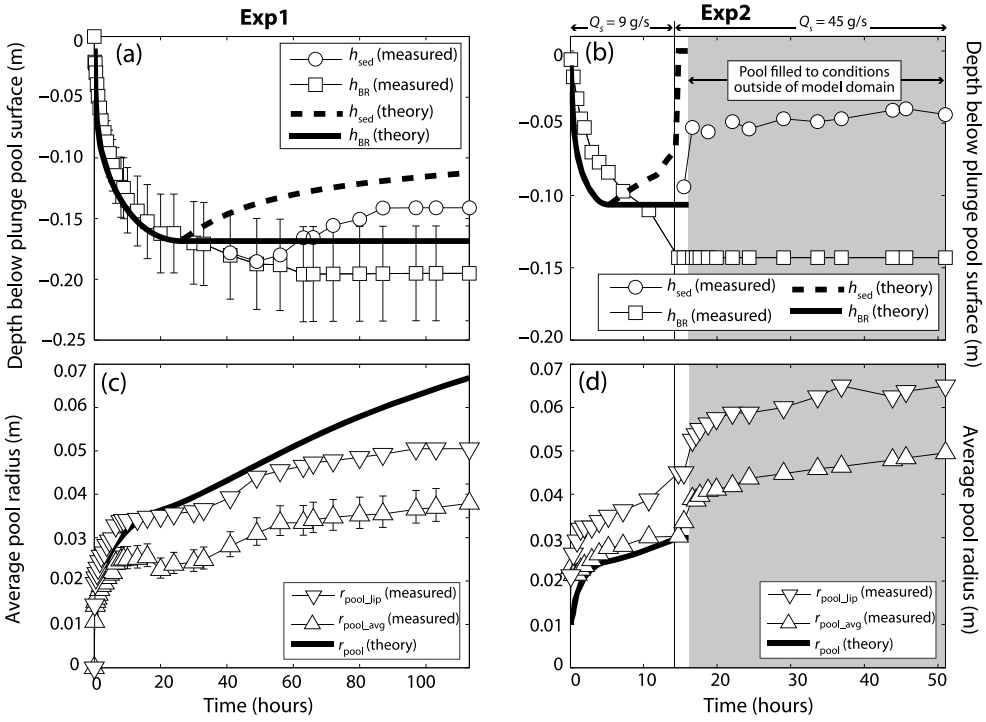


**Figure 3.** Comparison of theory-predicted and experimentally measured (Scheingross et al., 2017) plunge pool depth to bedrock ($h_{BR}$) and depth to sediment ($h_{sed}$) in (a) Exp1 and (b) Exp2, as well as comparisons of plunge pool radius in (c) Exp1 and (d) Exp2. Theory predictions were made allowing the pool depth and radius to co-evolve following equations (6a) and (6b) using 200 logarithmically spaced time steps spread over the experiment length (113 and 51 h in Exp1 and Exp2, respectively). $h_{sed}$ is shown only for cases when $h_{sed} \neq h_{BR}$ (i.e., periods when sediment was deposited or predicted to be deposited in the pool) in Figures 3a and 3b; error bars in Figures 3a and 3c reflect ~20% uncertainty in laser scanner measurements (Scheingross et al., 2017). Figures 3c and 3d show experimentally measured plunge pool radii measured at the top of the pool ($r_{pool\_lip}$) and averaged radii based on pool volume ($r_{pool\_avg}$; Scheingross et al., 2017). Thin, solid vertical line in Figures 3b and 3d denotes timing of sediment supply ($Q_s$) increase in Exp2, and gray shading denotes time when pool filled to levels outside of the model domain and no predictions are made.

reduction in sediment transport capacity. Eventually, the pool sediment transport capacity falls below the imposed sediment supply, and an alluvial cover develops on the pool floor, halting vertical incision. Thus, the maximum plunge pool depth to bedrock is set by the sediment transport capacity of the pool. Finally, the alluvial cover thickens until an equilibrium is reached between sediment transport capacity and the imposed supply (Scheingross & Lamb, 2016). Lateral erosion and pool widening continues after pool alluviation, and although not observed experimentally due to slow lateral abrasion rates, the maximum plunge pool radius is reached when the pool fills to its brim with sediment.

The theory predicts that evolving plunge pools have initially high vertical erosion rates, due to high-velocity particle impacts, which slow with time as pools grow deeper (Figure 3), similar to experimental observations. The model predicts pool radii that initially fall below $r_{min}$, and therefore, the pool radius first evolves following equation (13), and then later (when $r > r_{min}$), the pool radius evolves following the lateral abrasion model. Lateral erosion rates are predicted to slow with pool growth, primarily due to decreasing particle impact velocities and the increase in pool-wall surface area as pools grow.

In Exp2 the theory predicts the onset of alluviation earlier than in Exp1 because of the larger grain size and reduced plunge pool sediment transport capacity. In Exp1, alluviation occurs in the theory when the pool depth and radii are within ~15% of the experimentally observed values for the onset of sediment deposition, better agreement than typically observed in separate experiments used to test the plunge pool sediment transport capacity model (Scheingross & Lamb, 2016; Figure 3a). In Exp2, the theory predicts alluviation during the initial low-sediment supply period; however, sediment cover was not observed until later in this experiment when sediment supply was increased (Figure 3b), and this discrepancy is likely a result of uncertainty in the sediment transport capacity model.

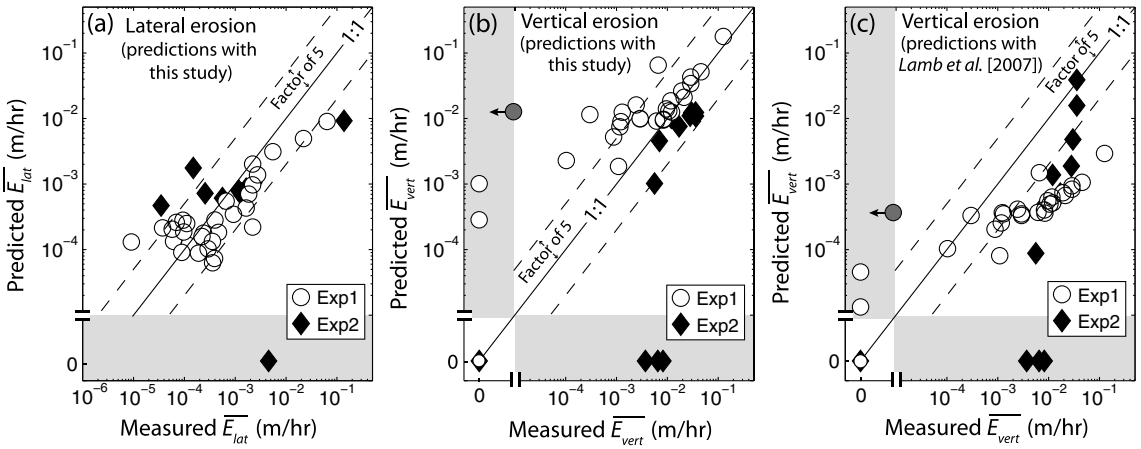


**Figure 4.** Comparison of experimentally measured (Scheingross et al., 2017) versus theoretically predicted (a) depth-averaged lateral erosion rate ($\overline{E_{lat}}$) and (b, c) area-weighted vertical erosion rate ($\overline{E_{vert}}$) for Exp1 and Exp2. Predictions in Figures 4a and 4b use the model developed here, and predictions in Figure 4c use Lamb et al. (2007). Solid line shows 1:1 prediction, and dashed lines show factor of 5 deviation. All predictions use experimentally measured values of average plunge pool radius ($r_{pool\_avg}$) and depth to bedrock (Scheingross et al., 2017). Points within the gray shaded box represent cases of zero erosion when theory and measurements disagree on the timing and level of sediment deposition within the pool. In Figures 4b and 4c, shaded circle with arrow represents a point in Exp1 when vertical erosion was below the detection limit in Scheingross et al. (2017). We omitted predictions for lateral erosion in Exp2 when pools filled to levels outside of the model domain.

The predictions of plunge pool depth to bedrock match observations within 25% in both experiments (Figures 3a and 3b), while predictions of plunge pool radius evolution match experimental measurements within a factor of 2 or better (Figures 3c and 3d). The theory matches observed instantaneous vertical and lateral erosion rates within a factor of ~5 (Figures 4a and 4b); cases where predictions depart by significantly more than a factor of 5 (within the shaded regions on Figure 4) correspond to times when the model incorrectly predicts pool alluviation. Using the Lamb et al. (2007) theory to predict vertical pool erosion results in systematic underprediction of erosion rates, with only 9 of 38 predictions matching measurements within a factor of 5 (compared to 23 of 38 using the model developed here; Figures 4b and 4c).

### 3.2. Controls on Plunge Pool Vertical and Lateral Erosion

Having tested the model against controlled experiments, we now explore the influence of changing plunge pool geometry, waterfall height, sediment size, water discharge, and sediment supply on model predictions of plunge pool vertical and lateral erosion rates. For all evaluations, we vary a single parameter while holding all other variables constant at representative values for the Fox Creek reference site.

#### 3.2.1. Pool Depth and Radius

With all else held constant for conditions at Fox Creek, increasing plunge pool depth to bedrock decreases the predicted plunge pool vertical erosion rate until $h_{BR} \approx 14$ m, after which sediment supply drops below plunge pool sediment transport capacity forcing alluviation and halting vertical erosion (Figure 5a). Similarly, plunge pool lateral erosion rates decrease with increasing pool depth until pools approach their maximum $h_{BR}$, after which lateral erosion rates increase.

The trends in erosion rate with changing pool depth occur because changes in $h_{BR}$ drive changes in sediment concentration, particle impact velocity, and the presence of sediment cover (equations (5a) and (5b)). For shallow plunge pools (when the pool bedrock floor lies within the ZOFE) with constant sediment supply, vertical plunge pool erosion rates are insensitive to depth because erosion is dominated by impacts from grains falling from the top of the waterfall that have a near constant impact velocity. In contrast, depth-averaged lateral erosion rates initially decrease with depth primarily because of averaging the same number of impacts over deeper pools with larger pool-wall area (equation (6b); Figure 5a). As pools deepen into the ZOEF, vertical impact velocities decrease, and the near-bed sediment concentration increases because deeper pools require higher near-bed sediment concentrations to transport the same sediment flux up and out of the pool. Eventually, the reduced vertical impact velocities and the onset of patchy sediment cover cause vertical incision rates to decrease. In contrast, lateral erosion rates increase with pool deepening as the influence of

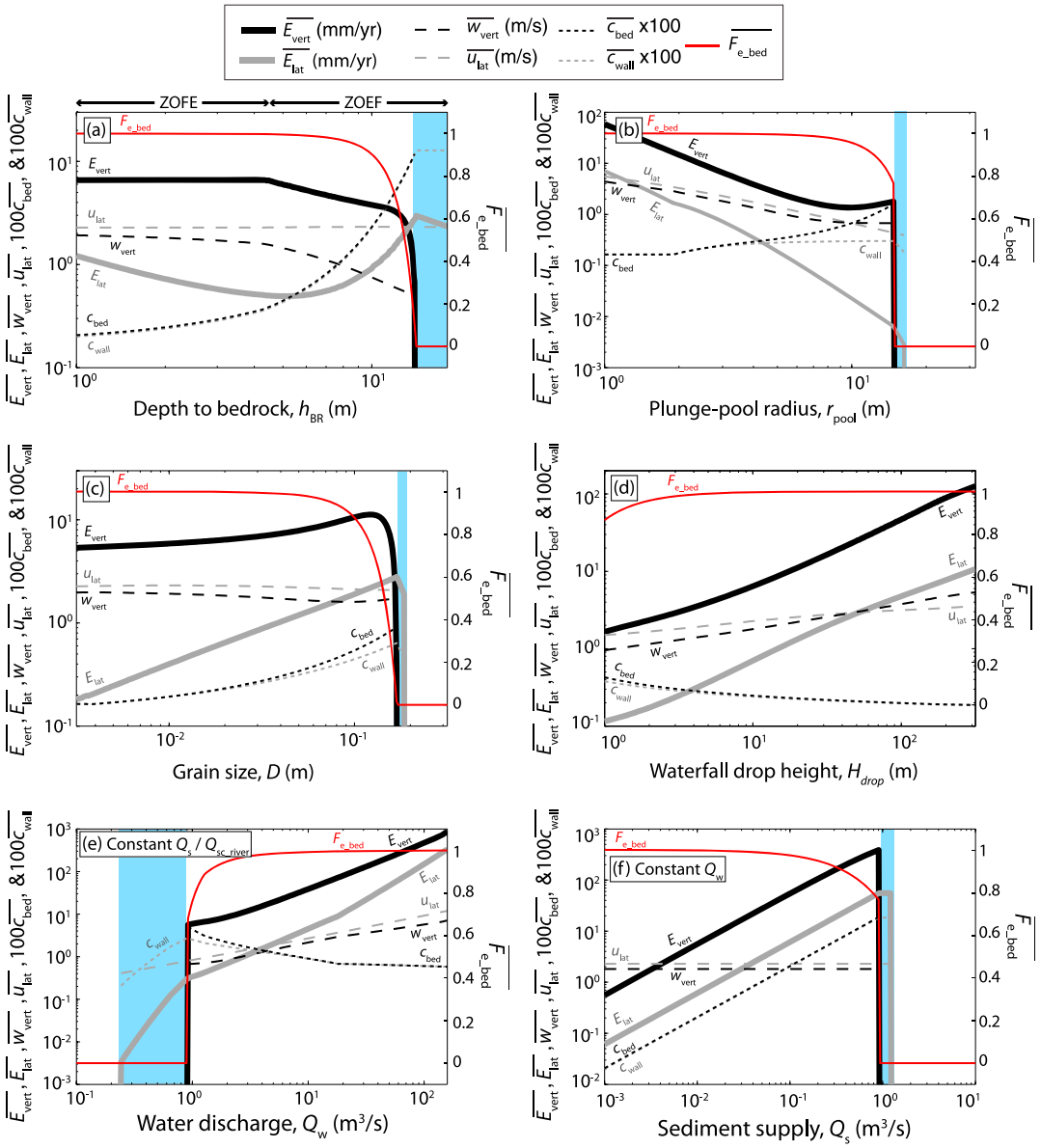


**Figure 5.** Model predictions of plunge pool erosion under changing (a) plunge pool depth to bedrock ($h_{BR}$), (b) plunge pool radius ($r_{pool}$), (c) grain size ($D$), (d) waterfall drop height ($H_{drop}$), (e) water discharge ($Q_w$), and (f) sediment supply ($Q_s$). In Figure 5e, the ratio of sediment supply to river sediment transport capacity is held constant at $Q_s/Q_{sc\_river} = 0.5$. In all panels, light blue shading denotes period when pool is partially filled with sediment ($z_{BR} < z_{sed} < z_{lip}$) such that pools can erode laterally, but there is no vertical erosion. All parameters other than those explicitly varied are held constant at reference values for Fox Creek ($Q_w = 7.2$ $m^3$/s, $Q_s = 0.01$ $m^3$/s, $h_{BR} = 2$ m, $r_{pool} = 3$ m, $H_{drop} = 10.4$ m, $D = 0.024$ m, $\sigma_T = 7$ MPa). $\overline{E_{vert}}$ is the area-weighted plunge pool vertical erosion and scales with the area-weighted near-bed sediment concentration ($\overline{c_{bed}}$), vertical impact velocity ($\overline{w_{vert}}$), and fraction of exposed bedrock on the bed ($\overline{F_{e\_bed}}$). $\overline{E_{lat}}$ is the depth-averaged lateral erosion rate and scales with the sediment concentration and lateral impact velocity averaged over the mixed layer ($\overline{c_{wall}}$ and $\overline{u_{lat}}$, respectively). Double-ended arrows in Figure 5a distinguish between the zone of flow establishment (ZOFE) and zone of established flow (ZOEF).

increasing near-bed sediment concentration on the walls outweighs the averaging over deeper pools (Figure 5a).

Similar to plunge pool depth, increasing plunge pool radius with all else held constant yields generally decreasing vertical and lateral erosion rates up until $r_{pool} \approx 15$ m after which sediment supply exceeds transport capacity and pools alluviate (Figure 5b). Decreases in vertical erosion rate with increasing radius occur

primarily due to averaging the same number of particle impacts of grains falling from the top of the waterfall over progressively larger bed surface areas (equation (6a)). Vertical erosion rates temporarily spike immediately prior to alluviation due to increasing near-bed sediment concentration, which occurs because wider pools require higher near-bed sediment concentrations to transport the imposed sediment supply up and out of the pool. The decrease of lateral erosion rates with increasing radius occurs due to reduced lateral impact velocity, which offsets increased sediment concentration near the wall (Figure 5b). At $r_{pool} \approx 15$, the pool alluviates and lateral erosion continues on the pool sidewalls until $r_{pool} \approx 17$, after which the pool is predicted to aggrade to its brim with sediment (Figure 5b). These model results are similar to our previously proposed conceptual model and experimental observations (Scheingross et al., 2017) and highlight how the plunge pool erosion model can be used to predict maximum plunge pool depths and radii for a given sediment supply and characteristic water discharge.

#### 3.2.2. Grain Size and Waterfall Height

Increasing grain size results in a higher particle settling velocity and reduces the jet's ability to transport sediment. When all else is held constant, the reduced transport efficiency of large grains causes higher near-bed sediment concentration in order to transport the imposed sediment supply. This increase in sediment concentration leads to faster vertical and lateral erosion rates because of a higher frequency of impacts, until the point where sediment supply approaches transport capacity (Figure 5c). For conditions at Fox Creek, the model predicts that vertical erosion rates decrease for $D > 12$ cm due to the onset of patchy cover over the bed (i.e., $F_{e\_bed} < 1$). Lateral erosion rates decrease once the pool alluviates ($D > 17$ cm) as it becomes easier to transport sediment in shallow plunge pools, thus reducing near-wall sediment concentration for the same sediment supply. For $D > 19$ cm, the pool completely fills with sediment, covering the pool walls and halting lateral erosion (Figure 5c).

Plunge pool vertical and lateral erosion rates are predicted to increase with increasing waterfall drop height (Figure 5d). This occurs because larger drop heights yield higher vertical and lateral particle impact velocities both through the energy gained from particles falling from higher heights (which increases $w_{vert}$) and increases in the waterfall jet velocity with height (which increases $w_{vert}$ and $u_{lat}$; Figure 5d). Increased waterfall jet velocity also increases bed shear stress and turbulent mixing ($L_d$), allowing for more efficient transport of grains out of the plunge pool. For a constant sediment supply, higher $\tau_b$ and $L_d$ reduce the near-bed sediment concentration and therefore particle impact rate; however, this has a small impact on erosion compared to the changes in particle impact velocity.

#### 3.2.3. Water Discharge and Sediment Supply

Both vertical and lateral erosion rates are predicted to increase with increasing water discharge and sediment supply with all else held constant (Figures 5e and 5f). Increasing sediment supply under constant discharge leads to higher sediment concentrations and particle impact rates, driving increased vertical and lateral erosion until sediment supply exceeds the plunge pool transport capacity, forcing alluviation and halting erosion (Figure 5f).

#### 3.2.4. Vertical Versus Lateral Erosion Rates

In almost all cases, the model predicts that vertical plunge pool erosion outpaces lateral erosion by approximately an order of magnitude or more. This imbalance occurs primarily because particles falling from the waterfall brink have high impact velocities and therefore typically produce more erosion per impact than the laterally directed impacts that occur on pool sidewalls. An exception to this rationale is when pools develop patchy or full alluvial cover and vertical erosion rates are reduced or are zero (Figure 5). For these cases, pools approach or achieve a transport-limited regime where near-wall sediment concentrations are high and lateral-wall erosion rates can be relatively large.

### 3.3. Knickzone Retreat Rate From Plunge Pool Drilling

Here we explore four separate cases of upstream knickzone retreat designed to approximate the influence of changing climate, tectonics, and waterfall formation in different ways by coupling our plunge pool erosion theory with a kinematic knickpoint retreat model (equation (32); Lamb et al., 2007). In the first case, we covary water discharge and sediment supply by holding the ratio of sediment supply relative to river sediment transport capacity, $Q_s/Q_{sc\_river}$, constant at 0.5, where $Q_{sc\_river}$ is calculated using Fernandez Luque and van Beek (1976). This scenario might approximate the influence of floods or long-term changes in climate as water discharge and sediment supply tend to covary in rivers (e.g., Leopold et al., 1964). The model predicts zero

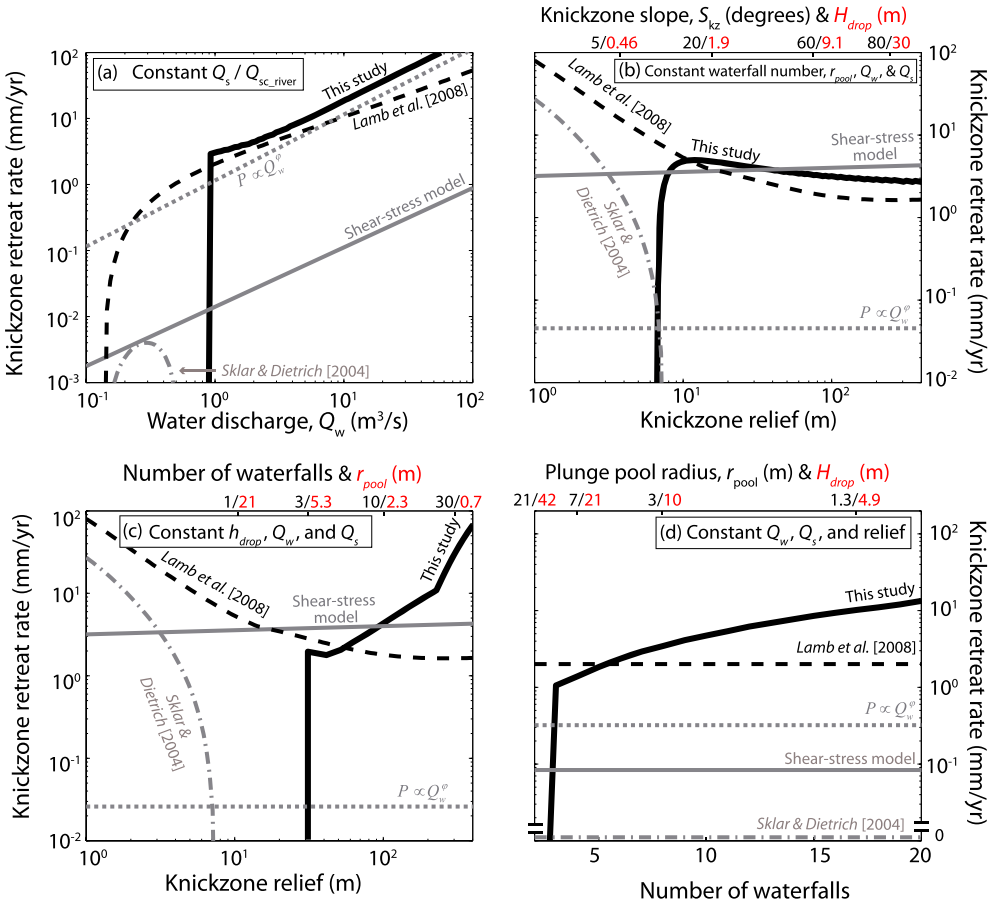


**Figure 6.** Comparison of the waterfall retreat model developed in this study versus low-gradient river incision models, which are commonly applied to predict knickzone retreat. (a) Predictions of retreat rate as a function of water discharge ($Q_w$) while holding the ratio of sediment supply ($Q_s$) to river sediment transport capacity ($Q_{sc\_river}$) constant at $Q_s/Q_{sc\_river}$ = 0.5, and (b) predictions of retreat rate for varying knickzone relief by varying waterfall drop height ($H_{drop}$) while holding knickzone length and all else constant such that higher relief results in steeper knickzones. (c) Same as Figure 6b except that knickzone relief is varied by changing the number and spacing of waterfalls while holding waterfall drop height and all else constant. (d) Predictions of retreat rate by covarying the number, spacing, and drop height of waterfalls while maintaining constant knickzone relief and length. Note that the saltation–abrasion model (Sklar & Dietrich, 2004) predicts zero erosion for all cases in Figure 6d owing to the steep knickzone slope. All parameters other than those explicitly varied were set constant at the Fox Creek reference site values ($Q_w$ = 7.2 m$^3$/s, $Q_s$ = 0.01 m$^3$/s, $h_{BR}$ = 2 m, $r_{pool}$ = 3 m, $H_{drop}$ = 10.4 m, $D$ = 0.024 m, $\sigma_T$ = 7 MPa, $H_{kz}$ = 83 m, $S_{kz}$ = 63°). Note that the shear stress model was empirically calibrated to match estimates of basin-averaged erosion at the reference site.

vertical or lateral plunge pool erosion for low discharges (Figure 5e) and, in turn, zero knickzone retreat (Figure 6a), because the river sediment transport capacity exceeds that of the plunge pool, causing pools to fill with sediment. As discharge and sediment supply increase, plunge pool transport capacity increases faster than the river transport capacity, allowing pools to evacuate deposited sediment and scour to bedrock. Both the plunge pool vertical and lateral erosion rates (Figure 5e) and knickzone retreat rates (Figure 6a) increase with increasing water discharge and sediment supply due to higher particle impact velocities and rates of impacts. In comparison, both a simple linear scaling between retreat rate and discharge (equation (35)) and the shear stress model (equation (33)) approximately capture the behavior, but not necessarily the magnitude, of our more complex model once a threshold discharge is surpassed (Figure 6a). The saltation–abrasion model predicts a humped relation where retreat rates initially increase due to increased bed shear stress and sediment supply, before dropping to zero at modest discharges where the theory predicts grains are in suspension (Figure 6a). In contrast, the total load model allows for impacts from suspended grains and predicts monotonically increasing retreat rates with increasing discharge that better matches the plunge pool erosion theory.

In the second case, we vary knickzone relief while holding the number of waterfalls, knickzone length, and all else constant, such that knickzones with more relief are steeper and have larger waterfall drop heights, $H_{drop}$ (Figure 6b). This case might approximate how changes in base level (e.g., sea-level change) can influence escarpment retreat. As waterfall drop height and knickzone relief increase, our model predicts a humped function for knickzone retreat, where retreat rate rapidly increases after surpassing a threshold knickzone relief, then slowly declines as knickzones grow in height (Figure 6b, section 3.2.2). Knickzone retreat rates increase at low relief because plunge pool floors transition from a covered to a sediment-free state due to the increase in plunge pool sediment transport capacity with increasing $H_{drop}$. At higher knickzone relief, the increase in $E_{vert}$ associated with larger $H_{drop}$ is offset by the need for taller knickzones to erode larger volumes of material to achieve the same upstream retreat rate (equation (32)). In comparison, the shear stress model shows slightly increasing retreat rates with increasing relief due to the inferred increase in reach-average slope (Figure 6b). The saltation–abrasion and total load models show decreasing retreat rates with increasing relief, which, for the total load model, is in agreement with the plunge pool erosion model for $H_{kz} > \sim$10 m (Figure 6b). In contrast, the simple discharge scaling relation (equation (35)) predicts no change in retreat rate with relief.

Within the context of the drilling model, the waterfall number and spacing should be set by the creation of new waterfalls just upstream of the escarpment. While this process has not been investigated in detail, new waterfalls may be created by instabilities such as cyclic steps that can form in the high Froude-number drawdown zone upstream of waterfall escarpments (Haviv et al., 2006; Scheingross, 2016; Yokokawa et al., 2013). Because cyclic step wavelength is predicted to decrease with reach-averaged bed slope (Brooks, 2001; Izumi et al., 2017), an increase in knickzone relief may also result in knickzones with more closely spaced waterfalls. We explore this scenario by varying knickzone relief while holding knickzone length, waterfall drop height, and all else constant. Thus, for low-relief knickzones, there are few waterfalls spaced far apart (i.e., large $r_{pool}$, small $m$), and for high-relief knickzones, waterfalls are numerous and closely spaced (small $r_{pool}$, large $m$; Figure 6c). Under this scenario, predictions of the shear stress, saltation–abrasion, and total load models remain unchanged from Figure 6b because these models depend on slope but are independent of waterfall spacing and number. For short, low-gradient escarpments, our model predicts retreat rates of zero because waterfalls have large plunge pool radii such that the imposed sediment supply exceeds sediment transport capacity and pools fill with sediment. As knickzone relief increases, closer spaced pools with smaller radii empty of sediment and particle impacts are concentrated over a smaller area, thus increasing the plunge pool erosion. Furthermore, the larger number of waterfalls allows for this enhanced erosion to occur over a greater portion of the escarpment, further increasing knickzone retreat rate (larger $m$ in equation (32)).

Finally, we explore how changes in waterfall number, spacing, and drop height influence knickzone retreat rate independent of changes in other parameters. We vary the number of waterfalls in a knickzone while holding knickzone relief, length, and slope constant, such that knickzones with more waterfalls have smaller drop heights and smaller radii (Figure 6d). Under this scenario, our model behaves similarly to the above case (Figure 6c). Retreat rates are zero when knickzones have less than three waterfalls because the large pool radii result in $Q_{sc\_pool} < Q_s$. With increasing number of waterfalls, retreat rates increase because of both the larger $m$ in equation (32)) and the smaller $r_{pool}$ that concentrate sediment impacts; these effects outweigh the influence of reduced impact velocities associated with shorter waterfalls (section 3.2.2; Figure 6d). In contrast, all the other erosion models predict constant erosion rates because they do not explicitly include the number of waterfalls in a knickzone.

## 4. Discussion

### 4.1. Limitations and Simplifications of the Model

The plunge pool erosion model presented here produces erosion rates that typically match experimental observations within a factor of ~5 and plunge pool depths to bedrock and radii that typically match observations within a factor of ~2 or better (Figures 3 and 4). The model tends to predict vertical pool erosion rates better than lateral erosion rates. This tendency may occur because vertical erosion is driven primarily by impacts from grains falling from the waterfall brink, such that the number and velocity of grain impacts, which drive erosion, depend on sediment supply and waterfall height. Lateral erosion, on the other hand, is driven by turbulent jets within the pool and more complex plunge pool hydraulics and sediment

transport. The largest mismatch occurs when the model incorrectly predicts the onset of alluviation, which stems from uncertainty in the sediment capacity model (Scheingross & Lamb, 2016), such that the model uncertainty is less for waterfalls that remain either fully covered or free of cover. Nonetheless, the mismatch between the theory and experiments is within the range of variability observed in simplified replicate bedrock erosion experiments (Scheingross et al., 2014; Sklar & Dietrich, 2001), which likely reflects the stochastic nature of turbulent flow, sediment transport, and evolving boundary conditions. The agreement between theory and experiments occurs despite the theoretical simplification of complex, three-dimensional, multiphase morphodynamics, and there was no tuning of free parameters within the theory to improve agreement with observations.

Our model assumes that the waterfall jet impacts at the center of the plunge pool floor and is formulated in terms of depth- and radially averaged erosion rates and a simplified cylindrical geometry. Discharge variability in nature likely causes the waterfall jet to sweep back and forth across the plunge pool, which may produce spatially uniform vertical lowering over long timescales. Nonetheless, our companion experiments showed lateral erosion concentrated on the downstream plunge pool wall (Scheingross et al., 2017). Developing theory capable of predicting spatially variable erosion will require new theory for plunge pool hydraulics and sediment transport under noncylindrical geometries.

Although the model is a simplified representation of natural waterfalls, there may be circumstances in which the model can be further simplified. Our theory suggests that pools rapidly transition between cover-free and alluviated states (Figure 5) such that applying a binary cover relation may be acceptable in many circumstances. The theory also predicts that vertical plunge pool erosion is dominated by grains that fall from the waterfall brink, owing to their high impact velocity relative to grains re-entrained from within the plunge pool. It seems therefore reasonable that vertical erosion could be predicted from a simplified model based on sediment supply (to constrain the number impacts) and the distance from the waterfall brink to the plunge pool floor (to constrain impact velocity). This approach is taken by Lamb et al. (2007); however, using their model results in poorer predictions of the experimental results (Figures 4b and 4c). Thus, the additional physics taken into account herein (e.g., accounting for drag produced by spatial variations in the waterfall jet (equations (17)–(23)) and accounting for spatial variations in impact velocity (equation (14)) and sediment concentration (equation (9)) when averaging impacts across the plunge pool floor (equation (6a)) appear to be necessary in cases. An attempt to simplify the lateral erosion model might also use sediment supply to constrain the number of impacts; however, estimating lateral impact velocity will still require some representation of jet hydrodynamics such as that included here.

### 4.2. Waterfall Retreat via Headwall Undercutting Versus Vertical Drilling

The plunge pool erosion model developed here is the first to describe both vertical and lateral plunge pool erosion, thus allowing evaluation of conditions when waterfall retreat should be dominated by headwall undercutting versus vertical drilling. Our results show that plunge pool vertical erosion tends to outpace lateral widening by almost an order of magnitude up until pools alluviate with sediment (Figure 5). Thus, until the point of pool alluviation, vertical drilling should be a more efficient retreat mechanism than headwall undercutting, in agreement with the flume experiments (Scheingross et al., 2017).

Plunge pool undercutting may be a generally ineffective mechanism to produce upstream waterfall retreat in homogenous rock. As pools widen, lateral erosion rates decrease nonlinearly making continued undercutting progressively more difficult (Figure 5b). In contrast, plunge pools can sustain vertically drilling if fluvial incision at the downstream plunge pool lip prevents pools from overdeepening and allows sediment to be flushed out of the pool (Scheingross et al., 2017). For the case of Fox Creek, fluvial incision at the downstream plunge pool lip is predicted to be ~1.4 mm/yr (using the total load model (Lamb et al., 2008) and assuming a 1% intermittency factor and $Fr = 1$ at the pool lip (Chow, 2009)). This downcutting rate is approximately a factor of 2 greater than the lateral erosion predicted by the plunge pool erosion model for the conditions at Fox Creek ($r_{pool} = 3$) and is orders of magnitude greater than the predicted pool lateral erosion rates at larger radii (Figure 5b).

Sediment transport and hydrodynamics limit the maximum radius that pools can achieve (section 3.2.1). For waterfalls to retreat via headwall undercutting, pool radii must extend across the sum of the horizontal distance between the waterfall jet and the headwall (Stein & Julien, 1993; Appendix B) and the critical distance

of headwall undercutting to produce failure. Evaluating these conditions using waterfalls from the Scheingross and Lamb (2016) database and using a well-established beam-bending caprock failure model (Haviv et al., 2010; Hayakawa & Matsukura, 2010; Timoshenko & Gere, 1978; Appendix B) shows that all surveyed waterfalls have pool radii less than that required for caprock failure (Table S1). Furthermore, 69 of the 75 waterfalls have theoretically maximum radii, predicted from the plunge pool model, that are less than that required for headwall caprock failure (Appendix B; Table S1). Lateral erosion rates are predicted to be larger if the base of the pool is composed of weaker rock, which could be due to a lithologic change or enhanced weathering from waterfall spray through wetting and drying or freeze/thaw cycles (Gilbert, 1896; Haviv et al., 2010). Nonetheless, while a weaker basal layer is easier to erode laterally, a stronger caprock requires more significant undercutting to fail because the critical undercutting distance for failure scales with caprock tensile strength (Haviv et al., 2010; Hayakawa & Matsukura, 2010; Timoshenko & Gere, 1978). Thus, while strong-over-weak stratigraphy may promote undercutting, it might not result in faster waterfall retreat that requires both undercutting and caprock failure.

For plunge pools formed in homogenous rock where the downstream plunge pool lip is free of sediment cover, the combination of model predictions of high vertical plunge pool erosion rates, downstream plunge pool lip lowering outpacing lateral plunge pool erosion, and limits on maximum plunge pool radius suggest that waterfall retreat should be driven primarily via vertical drilling rather than headwall undercutting. We suggest that plunge pools may evolve to a state near the threshold of cover, whereby pools rapidly drill to the onset of cover, and then go through cycles of downstream lip lowering, sediment removal, and continued vertical incision, similar to suggestions made for lowering of fluvial potholes (Johnson et al., 2010). For cases when downstream lip lowering is the rate-limiting step for continued plunge pool drilling, the average plunge pool depth to bedrock should be predictable from sediment transport theory (Scheingross & Lamb, 2016) based on the critical depth for onset of sediment cover. Furthermore, the lowering rate of the downstream plunge pool lip, rather than plunge pool vertical erosion rate, may be the rate-limiting control on waterfall retreat. For waterfalls in series (Figure 1b), it is also possible that lateral erosion of the downstream plunge pool wall can create small openings or "keyholes" in the next-most-downstream waterfall face (Cleland, 1910; Elston, 1917; Scheingross et al., 2017). These keyholes provide a spillover point below the plunge pool lip and allow sediment to be flushed out of the pool and continued vertical pool erosion.

### 4.3. Knickzone Retreat and Landscape Evolution

Knickzone retreat rates predicted by our model can differ significantly from rates predicted by fluvial erosion theories commonly applied to knickzones, which has important implications for our understanding of landscape response to changes in climate and tectonics (e.g., Lague, 2014; Whipple & Tucker, 2002; Whittaker, 2012; Wobus et al., 2010). Most commonly, rivers are assumed to respond to changes in forcing following stream power or celerity (e.g., equation (1)) models, and some workers use these models to infer the tectonic history of a catchment over millions of years from river profile analysis (e.g., Fox et al., 2014; Goren et al., 2014; Roberts & White, 2010). Our model suggests that for knickzones composed primarily of waterfalls, a shear stress or celerity-based model may capture the correct trends of knickzone retreat, if properly calibrated and with $\phi = 1$, but only in the scenario of changing water discharge and sediment supply in concert with all else held constant (Figure 6a) and, even for this scenario, only for large water discharges that exceed the threshold for erosion. If water discharge and sediment supply do not covary, then our model can deviate significantly from the shear stress approach both in trend and in magnitude.

More importantly, a crucial assumption in most river profile analyses used to infer tectonic history is that steeper rivers erode faster, which is central to the shear stress or stream power approach. However, our model predicts that the relationship between knickzone retreat rate and knickzone slope is complex, with a strongly positive trend for low-relief knickzones that are near the threshold for erosion (Figure 6b). For higher relief knickzones, our model predicts a slightly decreasing knickzone retreat rate for steeper sloping knickzones if the steeper knickzones have larger waterfall drop heights while holding the total number of waterfalls constant (Figure 6b). In contrast, if steeper knickzones have more waterfalls of similar height and smaller radii plunge pools, then the overall retreat rate is predicted to increase strongly with knickzone gradient and relief (Figure 6c). Thus, in a landscape evolution setting, our model would predict significantly different response times of landscapes to perturbations as compared to the shear-stress model, and the qualitative and quantitative response of the knickzone depends on the magnitude of external forcing and the internal dynamics of

the waterfall system (i.e., the number, spacing, and height of waterfalls in the knickzone). Thus, inverse methods that attempt to reconstruct long-term uplift history from river profile shape may encounter significant problems in catchments with waterfalls.

The saltation–abrasion model has been used to explain the origin of hanging valleys that do not retreat (e.g., Crosby et al., 2007; Goode & Burbank, 2009; Wobus et al., 2006), and it may also generate sustained relief in landscape evolution models after the cessation of tectonic forcing (Egholm et al., 2013). The saltation–abrasion model produces this behavior at steep knickzones because beyond a threshold water discharge (Figure 6a) or slope (Figure 6b), it predicts that erosion rates are zero as particle hop lengths tend to infinity. The saltation–abrasion model was not designed to be used in steep knickzones. For knickzones composed of waterfalls, our model predicts the opposite behavior—that knickzones continue to retreat, and often retreat faster, in response to heightened relief (Figures 6b and 6c), implying that knickzones may not stall to produce hanging valleys. In fact, in most of the parameter space explored in Figure 6, our waterfall model predicts finite erosion only where the saltation–abrasion model predicts zero erosion. This occurs because the threshold for waterfall erosion, in many cases, exceeds the threshold for suspension and assumed infinite hop lengths in the saltation–abrasion model. The total load model better matches our knickzone retreat model, but it fails to predict the threshold for erosion (Figures 6a and 6b) and diverges strongly from our model predictions for cases in which the number and spacing of waterfalls change (Figures 6c and 6d).

Our results highlight the importance of waterfall internal dynamics (i.e., waterfall spacing, height, and number) in setting knickzone retreat rates by successive, vertically drilling waterfalls (Figure 6) and points to a need to develop new theory capable of predicting waterfall formation, spacing, and number (e.g., Izumi et al., 2017) over landscape evolution timescales. Waterfall spacing and number have the same order of magnitude effect on knickpoint retreat rates within our model as changes in external forcing. Thus, accounting for waterfall processes can influence both the rate of adjustment and resulting morphology of landscapes responding to perturbations in climate and tectonics in ways that are currently not captured in landscape evolution models.

## 5. Conclusions

We developed a model to predict rates of plunge pool vertical and lateral erosion via particle abrasion, building on previously developed models for plunge pool sediment transport capacity (Scheingross & Lamb, 2016) and fluvial bedrock incision (Lamb et al., 2007; Lamb et al., 2008; Sklar & Dietrich, 2004). Our model predicts similar behavior to that observed in experiments with eroding plunge pools in homogeneous rock with fixed downstream pool lips, where pools have initially rapid vertical and lateral incision rates, which slow as pools deepen and particle impact velocities decrease. The model reproduces plunge pool depths and radii that agree with experimental observations within a factor of 2. Under constant forcing, the model predicts that plunge pool vertical incision outpaces lateral erosion by almost an order of magnitude, such that developing pools vertically drill and deepen until sediment supply exceeds sediment transport capacity, forcing sediment deposition on the pool floor that halts vertical incision. After deposition, lateral erosion persists, albeit at rates that are low relative to predictions of fluvial incision on the downstream plunge pool lip, such that downstream lip lowering likely allows pools to export deposited sediment and continue incising vertically. Our results suggest that at least in homogeneous rock, upstream knickzone retreat is likely to be driven by vertical drilling of successive waterfall plunge pools rather than the classic headwall undercutting mechanism. The model predicts that knickzones composed of drilling waterfalls retreat upstream faster for cases of large covarying water discharge and sediment supply and for knickzones with more abundant and closely spaced waterfalls. Our model indicates that knickzones respond to changes in tectonics and climate in ways that differ significantly, both qualitatively and quantitatively, from existing low-gradient fluvial incision rules that are commonly applied in landscape evolution models and inverse methods to reconstruct tectonic history from river profile shape.

## Appendix A

Here we evaluate the reasonableness of the assumption that lateral impacts occur when suspended grains have sufficient inertia to detach from the fluid and impact the wall by examining a ratio of characteristic length scales. We approximate the length over which particles slow in the absence of a lateral jet using an

e-folding distance for fluid-drag-induced particle slowing, $l_{e\_fold}$, and compare this to the length scale over which jets turn vertically, which we represent with the radial jet half width at the pool wall, $b_{lat}(r_{pool})$ (Figure 2). When $l_{e\_fold}/b_{lat}(r_{pool}) > 1$, particles should have sufficient inertia to impact the wall after detaching from the flow, whereas when $l_{e\_fold}/b_{lat}(r_{pool}) < 1$, particles will slow significantly after detaching from the flow, reducing lateral impact velocity.

We calculate $l_{e\_fold}$ using conservation of momentum to solve for the deceleration of a particle with lateral velocity $u(r)$ due to drag in the absence of other forces, for example,

$$\frac{du(r)}{dt} = -\frac{1}{2} C_{drag} \frac{\rho_f}{\rho_s} \frac{A_p}{V_p} u(r)^2, \tag{A1}$$

where the right-hand side of equation (A1) is the drag force normalized by particle mass. Substituting $dt = dr/u(r)$ into equation (A1) and rearranging gives a first-order differential equation equivalent to the exponential decay equation

$$\frac{du(r)}{dr} = -\frac{1}{2} C_{drag} \frac{\rho_f}{\rho_s} \frac{A_p}{V_p} u(r). \tag{A2}$$

The e-folding length scale for particle stopping can be calculated by solving equation (A2) with a boundary condition of $u(r_{pool}) = u_{lat}$, substituting $u(l_{e\_fold})/u_{lat} = 1/e$ and rearranging to yield

$$l_{e\_fold} = \frac{2}{C_{drag}} \frac{\rho_s}{\rho_f} \frac{V_p}{A_p} = 3.6 \frac{D}{C_{drag}}, \tag{A3}$$

where we have assumed spherical grains and sediment with $\rho_s$ = 2,650 kg/m$^3$.

Combining equations (29) and (A3), the ratio of $l_{e\_fold}$ to $b_{lat}(r_{pool})$ can be calculated as

$$\frac{l_{e\_fold}}{b_{lat}(r_{pool})} = \frac{40D}{C_{drag} r_{pool}}. \tag{A4}$$

Using the database of natural plunge pools surveyed by Scheingross and Lamb (2016) and setting $C_{drag}$ to a conservative value of unity (Ferguson & Church, 2004) yield a median value of $l_{e\_fold}/b_{lat}(r_{pool})$ of 1.9 with ~63% of surveyed pools having $l_{e\_fold}/b_{lat}(r_{pool}) > 1$ (Table S1). This suggests that our assumption that laterally advected particles can detach from the flow to impact the sidewalls is reasonable across the majority of surveyed plunge pools. This assumption likely breaks down high on pool walls where radial wall jets have slow velocities and vertical wall jets are thick; therefore, we exclude impacts for $z > z_{mixed}$ in our theory.

## Appendix B

Here we develop a theory for the maximum radius to which plunge pools can grow by applying constraints based on criteria for caprock failure and the filling of pools with sediment. For waterfalls to retreat by headwall undercutting, plunge pools must be able to undercut a critical distance, $l_{crit}$, from the waterfall base in order to produce caprock failure. We define a critical plunge pool radius, $r_{crit}$, for caprock failure as

$$r_{crit} = l_{jet} + l_{crit}, \tag{B1}$$

where $l_{jet}$ is the horizontal distance between the waterfall face and the point where the waterfall jet impacts the plunge pool floor and can be solved following the standard plunge pool hydraulic theory (Stein & Julien, 1993):

$$l_{jet} = u_{brink} \left( \frac{2(z_{brink} - z_{sed})}{g} \right)^{1/2}. \tag{B2}$$

We solve for $l_{crit}$ with a 2-D tensile strength beam failure model (e.g., Haviv et al., 2010; Hayakawa & Matsukura, 2010; Timoshenko & Gere, 1978), assuming all undercutting occurs within the plunge pool:

$$l_{crit} = \left( \frac{\sigma_t [z_{brink} - z_{water}]}{3\rho_s g} \right)^{1/2}. \tag{B3}$$

As plunge pools may be actively eroding and widening, we use the radius at which a pool completely fills with sediment (i.e., $z_{lip} = z_{sed}$; Figure 2) as a conservative estimate of the maximum plunge pool radius, $r_{max}$, and solve for $r_{max}$ with recently developed plunge pool sediment transport capacity theory (Scheingross & Lamb, 2016).

The ratio of $r_{max}/r_{crit}$ defines a criterion to evaluate the potential for retreat by undercutting, whereby retreat requires $(r_{max}/r_{crit}) \geq 1$. We evaluate $r_{max}/r_{crit}$ using waterfalls from the Scheingross and Lamb (2016) database (Table S1), assuming a 2-year recurrence water discharge, setting $Q_s = 0$ to give the maximum possible radius, using the median grain size found in the channel reach, and using a conservative value for tensile strength ($\sigma_t$ = 5 MPa; Sklar & Dietrich, 2001) for the crystalline rocks in which the waterfalls from the database are predominately found. Note that in some cases field-measured plunge pool radii are greater than $r_{max}$ predicted with the above methods (Table S1). This could occur, for example, if plunge pool radii are set by floods larger than the 2 year recurrence interval discharge or by sediment smaller than the median grain size in the reach. For example, estimating $r_{max}$ using the plunge pool rather than the channel reach median grain size (Scheingross & Lamb, 2016) results in $r_{max} > r_{pool}$ for all but one of the waterfalls in the Scheingross and Lamb (2016) database.

## Notation

| | |
|---|---|
| $A$ | drainage area [$L^2$] |
| $A_1$ | constant indicating fraction of particles impacting bedrock surfaces [dimensionless] |
| $A_{jdr}$ | area of the jet-descending region on the pool floor [$L^2$] |
| $A_p$ | particle cross-sectional area [$L^2$] |
| $A_{pool}$ | cross-sectional area of plunge pool floor [$L^2$] |
| $C_{drag}$ | drag coefficient [dimensionless] |
| $C_{f\_river}$ | river friction factor [dimensionless] |
| $D$ | grain diameter [L] |
| $E$ | volumetric erosion rate per unit bed area [L/T] |
| $E_{lat}(z)$ | plunge pool lateral erosion rate along pool walls [L/T] |
| $\overline{E_{lat}}$ | depth-averaged plunge pool lateral erosion rate [L/T] |
| $E_{river}$ | river vertical erosion rate [L/T] |
| $E_{vert}(r)$ | plunge pool vertical erosion rate along pool floor [L/T] |
| $\overline{E_{vert}}$ | area-averaged plunge pool vertical erosion rate [L/T] |
| $F_e$ | fraction of exposed bedrock [dimensionless] |
| $F_{e\_bed}(r)$ | fraction of bedrock exposed along plunge pool floor [dimensionless] |
| $F_{e\_wall}(z)$ | fraction of bedrock exposed along plunge pool walls [dimensionless] |
| $F_g$ | gravitational force [$ML/T^2$] |
| $F_{d\_jet}$ | drag force on the waterfall jet [$ML/T^2$] |
| $H_{drop}$ | waterfall drop height [L] |
| $H_{kz}$ | waterfall escarpment relief [L] |
| $I_r$ | particle impact rate per unit area [impacts/$L^2T$] |
| $K$ | constant in shear stress model [$L^2T/M$ if $a = 1$] |
| $L_d$ | characteristic length scale over which turbulence mixes sediment [L] |
| $P$ | knickzone retreat rate [L/T] |
| $Q_s$ | sediment supply [$L/T^3$] |
| $Q_{sc\_pool}$ | plunge pool sediment transport capacity [$L/T^3$] |
| $Q_{sc\_river}$ | river sediment transport capacity [$L/T^3$] |
| $Q_w$ | water discharge [$L/T^3$] |
| $S$ | reach-averaged channel slope [dimensionless] |
| $S_{kz}$ | reach-averaged knickzone slope [dimensionless] |
| $U$ | depth-averaged flow velocity [L/T] |
| $V_i$ | volume of bedrock eroded per particle impact [$L^3$/impact] |
| $V_p$ | particle volume [$L^3$] |
| $W$ | reach-averaged channel width [L] |

| | |
|---|---|
| $a$ | empirical exponent in shear stress erosion model [dimensionless] |
| $b(z)$ | half-width of the descending waterfall jet [L] |
| $b_{lat}(r)$ | half-width of the wall jet along the pool floor [L] |
| $c(r, z)$ | sediment concentration at point $(r, z)$ [dimensionless] |
| $c_o$ | near-bed sediment concentration |
| $c_b$ | well-mixed layer sediment concentration in the jet-descending region [dimensionless] |
| $c_{bed}(r)$ | sediment concentration along the plunge pool floor [dimensionless] |
| $\overline{c_{bed}}$ | area-weighted sediment concentration on the plunge pool floor [dimensionless] |
| $c_{bed\_capacity}(r)$ | well-mixed layer sediment concentration at transport capacity along the plunge pool floor [dimensionless] |
| $c_{wall}(z)$ | sediment concentration along the plunge pool wall [dimensionless] |
| $\overline{c_{wall}}$ | average sediment concentration along the pool wall in the mixed layer [dimensionless] |
| $c_{wf}$ | concentration of grains falling from the waterfall brink estimated on the pool floor [dimensionless] |
| $g$ | gravitational acceleration [$L/T^2$] |
| $h_{BR}$ | plunge pool depth to bedrock [L] |
| $h_n$ | river normal flow depth [L] |
| $h_{sed}$ | plunge pool depth to sediment [L] |
| $k$ | empirical constant in stream power style waterfall retreat model [$L^{(1-2\phi)}/T$] |
| $k_Y$ | empirical constant relating energy transfer and elasticity [$M/(LT^2)$] |
| $l_{crit}$ | threshold undercut distance for caprock failure [L] |
| $l_{e\_fold}$ | e-folding distance for slowing of laterally advected particles [L] |
| $l_{jet}$ | horizontal distance between waterfall face and point of jet impingement at the plunge pool floor [L] |
| $m$ | number of plunge pools within a knickzone not including the base [L] |
| $r$ | plunge pool radial coordinate [L] |
| $r_{crit}$ | threshold plunge pool radius for caprock failure [L] |
| $r_{jet}$ | waterfall jet radius at point of impact with water surface [L] |
| $r_{max}$ | maximum plunge pool radius set by sediment transport constraints [L] |
| $r_{min}$ | imposed minimum radius for plunge pools to maintain [L] |
| $r_{pool}$ | plunge pool radius [L] |
| $r_{pool\_avg}$ | average plunge pool radius from pool volume assume cylindrical geometry [L] |
| $r_{pool\_lip}$ | average plunge pool radius at $z_{lip}$ [L] |
| $t$ | time [T] |
| $u_{brink}$ | river water velocity at the upstream waterfall brink [L/T] |
| $u_{lat}(z)$ | particle lateral impact velocity along pool walls [L/T] |
| $\overline{u_{lat}}$ | particle lateral impact velocity averaged over the mixed layer [L/T] |
| $u_n$ | normal river flow velocity [L/T] |
| $u_s$ | saltation velocity [L/T] |
| $u_{wall}(r, z)$ | wall-jet velocity as a function of position [L/T] |
| $u_{wall\_max}$ | maximum wall-jet velocity at the plunge pool wall [L/T] |
| $w_i$ | vertical particle impact velocity [L/T] |
| $w_{jet}(r, z)$ | descending waterfall jet velocity as function of position [L/T] |
| $\overline{w_{jet}(z)}$ | radially averaged waterfall jet velocity [L/T] |
| $w_{net}$ | net particle settling velocity [L/T] |
| $w_{particle}(r, z)$ | velocity of a particle falling from the waterfall brink as function of position [L/T] |
| $w_s$ | terminal particle gravitational settling velocity [L/T] |
| $w_{up}$ | vertical velocity of the jet return flow [L/T] |
| $w_{vert}(r)$ | averaged vertical impact velocity for particles impacting the plunge pool floor [L/T] |
| $\overline{w_{vert}}$ | area-weighted vertical particle impact velocity [L/T] |
| $w_{vert\_susp}$ | vertical impact velocity of particles falling out of suspension [L/T] |
| $w_{vert\_wf}$ | vertical impact velocity of particles falling from the waterfall brink [L/T] |
| $z$ | plunge pool vertical coordinate [L] |
| $z_{BR}$ | elevation of the plunge pool bedrock floor [L] |

| | |
|---|---|
| $z_{brink}$ | elevation of the waterfall brink upstream of the plunge pool [L] |
| $z_{lip}$ | elevation of the downstream plunge pool lip [L] |
| $z_{mixed}$ | elevation of the top of the well-mixed sediment layer near the plunge pool floor [L] |
| $z_{sed}$ | elevation of the plunge pool alluvial floor [L] |
| $z_{water}$ | elevation of the water surface in the plunge pool [L] |
| $z_\lambda$ | elevation of the transition between the ZOEF and ZOFE [L] |
| $\beta$ | angle of waterfall jet impact [rad] |
| $\delta(z)$ | radius of the jet-descending region as a function of pool depth [L] |
| $\kappa$ | constant in bedrock erosion theory [$T^2/L^2$] |
| $\lambda$ | length of ZOFE [L] |
| $\phi$ | empirical constant in waterfall retreat model [dimensionless] |
| $\rho_f$ | fluid density [$M/L^3$] |
| $\rho_s$ | sediment or bedrock density [$M/L^3$] |
| $\rho_w$ | water density [$M/L^3$] |
| $\sigma_T$ | bedrock tensile strength [$M/(LT^2)$] |
| $\tau_b$ | river-bed shear stress [$M{\cdot}L^{-1}\,T^{-2}$] |
| $\chi$ | integral that accounts for vertical and radial decay of sediment concentration between the point of jet impingement on the plunge pool floor and lip [L] |

**Acknowledgments**
All data necessary to reproduce the results and figures in this manuscript are included in the supporting information or within our previously published work (Scheingross et al., 2017; Scheingross & Lamb, 2016). A MATLAB script to calculate plunge pool erosion is also included in the supporting information. We are grateful to Jeff Prancevic, Roman DiBiase, Andy Thompson, Jean-Philippe Avouac, Florent Gimbert, and Jens Turowski for stimulating discussions. Formal reviews from Dimitri Lague and two anonymous reviewers as well as editorial input from Joel Johnson and John Buffington improved the clarity and presentation of this manuscript. We acknowledge funding from the National Science Foundation via grant EAR-1147381 to M. P.L and a Graduate Research Fellowship to J.S.S., funding from NASA grant 12PGG120107 to M.P.L., and an Alexander von Humboldt Postdoctoral Fellowship to J.S.S.

## References

Abramovich, G., & Schindel, L. (1963). *The Theory of Turbulent Jets* (pp. 671). Cambridge, MA: MIT Press.

Albertson, M. L., Dai, Y. B., Jensen, R. A., & Rouse, H. (1950). Diffusion of submerged jets. *Transactions of the American Society of Civil Engineers*, *115*(1), 639–664.

Alonso, C. V., Bennett, S. J., & Stein, O. R. (2002). Predicting head cut erosion and migration in concentrated flows typical of upland areas. *Water Resources Research*, *38*(12), 1303. https://doi.org/10.1029/2001WR001173

Anton, L., Mather, A. E., Stokes, M., Munoz-Martin, A., & De Vicente, G. (2015). Exceptional river gorge formation from unexceptional floods. *Nature Communications*, *6*. https://doi.org/10.1038/ncomms8963

Baynes, E. R. C., Attal, M., Niedermann, S., Kirstein, L. A., Dugmore, A. J., & Naylor, M. (2015). Erosion during extreme flood events dominates Holocene canyon evolution in northeast Iceland. *Proceedings of the National Academy of Sciences of the United States of America*, *112*(8), 2355–2360. https://doi.org/10.1073/pnas.1415443112

Beltaos, S. (1976). Oblique impingement of plane turbulent jets. *Journal of the Hydraulics Division-Asce*, *102*(9), 1177–1192.

Beltaos, S., & Rajaratnam, N. (1973). Plane turbulent impinging jets. *Journal of Hydraulic Research*, *11*(1), 29–59. https://doi.org/10.1080/00221687309499789

Beltaos, S., & Rajaratnam, N. (1974). Impinging circular turbulent jets. *Journal of the Hydraulics Division-Asce*, *100*(10), 1313–1328.

Bennett, S. J., Alonso, C. V., Prasad, S. N., & Romkens, M. J. M. (2000). Experiments on headcut growth and migration in concentrated flows typical of upland areas. *Water Resources Research*, *36*(7), 1911–1922. https://doi.org/10.1029/2000WR900067

Berlin, M. M., & Anderson, R. S. (2009). Steepened channels upstream of knickpoints: Controls on relict landscape response. *Journal of Geophysical Research*, *114*, F03018. https://doi.org/10.1029/2008JF001148

Bishop, P., Hoey, T. B., Jansen, J. D., & Artza, I. A. (2005). Knickpoint recession rate and catchment area: The case of uplifted rivers in eastern Scotland. *Earth Surface Processes and Landforms*, *30*(6), 767–778. https://doi.org/10.1002/esp.1191

Bollaert, E., & Schleiss, A. (2003). Scour of rock due to the impact of plunging high velocity jets Part I: A state-of-the-art review. *Journal of Hydraulic Research*, *41*(5), 451–464. https://doi.org/10.1080/00221680309499991

Brocard, G. Y., Willenbring, J. K., Miller, T. E., & Scatena, F. N. (2016). Relict landscape resistance to dissection by upstream migrating knickpoints. *Journal of Geophysical Research: Earth Surface*, *121*, 1182–1203. https://doi.org/10.1002/2015JF003678

Brooks, P. C. (2001). *Experimental Study of Erosional Cyclic Steps*. Minnesota: University of Minnesota.

Chatanantavet, P., & Parker, G. (2006). Modeling the bedrock river evolution of western Kaua'i, Hawai'i, by a physically-based incision model based on abrasion. In G. Parker & M. Garcia (Eds.), *River, Coastal and Estuarine Morphodynamics 2005* (pp. 99–110). London: Taylor and Francis Group.

Chatanantavet, P., Whipple, K. X., Adams, M. A., & Lamb, M. P. (2013). Experimental study on coarse grain saltation dynamics in bedrock channels. *Journal of Geophysical Research: Earth Surface*, *118*, 1161–1176. https://doi.org/10.1002/jgrf.20053

Chow, V. T. (2009). *Open-Channel Hydraulics*. New Jersey: The Blackburn Press.

Cleland, H. F. (1910). North American natural bridges, with a discussion of their origin. *Geological Society of America Bulletin*, *21*(1), 313–338. https://doi.org/10.1130/GSAB-21-313

Crosby, B. T., & Whipple, K. X. (2006). Knickpoint initiation and distribution within fluvial networks: 236 waterfalls in the Waipaoa River, North Island, New Zealand. *Geomorphology*, *82*(1–2), 16–38. https://doi.org/10.1016/j.geomorph.2005.08.023

Crosby, B. T., Whipple, K. X., Gasparini, N. M., & Wobus, C. W. (2007). Formation of fluvial hanging valleys: Theory and simulation. *Journal of Geophysical Research*, *112*, F03S10. https://doi.org/10.1029/2006JF000566

DiBiase, R. A., & Whipple, K. X. (2011). The influence of erosion thresholds and runoff variability on the relationships among topography, climate, and erosion rate. *Journal of Geophysical Research*, *116*, F04036. https://doi.org/10.1029/2011JF002095

DiBiase, R. A., Whipple, K. X., Lamb, M. P., & Heimsath, A. M. (2015). The role of waterfalls and knickzones in controlling the style and pace of landscape adjustment in the western San Gabriel Mountains, California. *Geological Society of America Bulletin*, *127*(3–4), 539–559. https://doi.org/10.1130/B31113.1

Dietrich, W. E., Bellugi, D., Heimsath, A. M., Roering, J. J., Sklar, L., & Stock, J. D. (2003). In P. R. Wilcock & R. M. Iverson (Eds.), *Geomorphic Transport Laws for Predicting the Form and Evolution of Landscapes*, *Geophysical Monograph Series* (pp. 103–132). Washington, DC: American Geophysical Union. https://doi.org/10.1029/GM135

Egholm, D., Knudsen, M., & Sandiford, M. (2013). Lifespan of mountain ranges scaled by feedbacks between landsliding and erosion by rivers. *Nature*, *498*, 475–478. https://doi.org/10.1038/nature12218

Elston, E. D. (1917). Potholes: Their variety, origin and significance. *The Scientific Monthly*, *5*(6), 554–567.

Elston, E. D. (1918). Potholes: Their variety, origin and significance II. *The Scientific Monthly*, *6*(1), 37–51.

Ferguson, R. I., & Church, M. (2004). A simple universal equation for grain settling velocity. *Journal of Sedimentary Research*, *74*(6), 933–937. https://doi.org/10.1306/051204740933

Fernandez Luque, R., & van Beek, R. (1976). Erosion and transport of bed-load sediment. *Journal of Hydraulic Research*, *14*, 127–144. https://doi.org/10.1080/00221687609499677

Flores-Cervantes, J. H., Istanbulluoglu, E., & Bras, R. L. (2006). Development of gullies on the landscape: A model of headcut retreat resulting from plunge pool erosion. *Journal of Geophysical Research*, *111*, F01010. https://doi.org/10.1029/2004JF000226

Fox, M., Goren, L., May, D. A., & Willett, S. D. (2014). Inversion of fluvial channels for paleorock uplift rates in Taiwan. *Journal of Geophysical Research: Earth Surface*, *119*, 1853–1875. https://doi.org/10.1002/2014JF003196

Frankel, K. L., Pazzaglia, F. J., & Vaughn, J. D. (2007). Knickpoint evolution in a vertically bedded substrate, upstream-dipping terraces, and Atlantic slope bedrock channels. *Geological Society of America Bulletin*, *119*(3–4), 476–486. https://doi.org/10.1130/b25965.1

Gallen, S. F., Wegmann, K. W., Frankel, K. L., Hughes, S., Lewis, R. Q., Lyons, N., … Witt, A. C. (2011). Hillslope response to knickpoint migration in the Southern Appalachians: Implications for the evolution of post-orogenic landscapes. *Earth Surface Processes and Landforms*, *36*(9), 1254–1267. https://doi.org/10.1002/esp.2150

Garcia, M. H. (2008). Sediment transport and morphodynamics. In M. H. Garcia (Ed.), *Sedimentation Engineering: Processes, Measurements, Modeling, and Practice* (pp. 21–163). Reston, VA: American Society of Civil Engineers. https://doi.org/10.1061/9780784408148

Ghaneeizad, S. M., Atkinson, J. F., & Bennett, S. J. (2015). Effect of flow confinement on the hydrodynamics of circular impinging jets: Implications for erosion assessment. *Environmental Fluid Mechanics*, *15*(1), 1–25. https://doi.org/10.1007/s10652-014-9354-3

Giger, M., Dracos, T., & Jirka, G. H. (1991). Entrainment and mixing in plane turbulent jets in shallow-water. *Journal of Hydraulic Research*, *29*(5), 615–642. https://doi.org/10.1080/00221689109498980

Gilbert, G. K. (1890). The history of the Niagara River, extracted from the sixth annual report to the commissioners of the state reservation at Niagara, Albany, NY.

Gilbert, G. K. (1896). Niagara Falls and their history. In J. W. Powell (Ed.), *Physiography of the United States, National Geographic Society Monographs* (pp. 203–236). New York: American Book Co.

Gilbert, G. K. (1907). Rate of recession of Niagara Falls. *US Geological Survey Bulletin*, *306*, 1–31.

Goode, J. K., & Burbank, D. W. (2009). Numerical study of degradation of fluvial hanging valleys due to climate change. *Journal of Geophysical Research*, *114*, F01017. https://doi.org/10.1029/2007JF000965

Goren, L., Fox, M., & Willett, S. D. (2014). Tectonics from fluvial topography using formal linear inversion: Theory and applications to the Inyo Mountains, California. *Journal of Geophysical Research: Earth Surface*, *119*, 1651–1681. https://doi.org/10.1002/2014JF003079

Hager, W. H. (1983). Hydraulics of plane free overfall. *Journal of Hydraulic Engineering-Asce*, *109*(12), 1683–1697. https://doi.org/10.1061/(ASCE)0733-9429(1983)109:12(1683)

Haviv, I., Enzel, Y., Whipple, K. X., Zilberman, E., Matmon, A., Stone, J., & Fifield, K. L. (2010). Evolution of vertical knickpoints (waterfalls) with resistant caprock: Insights from numerical modeling. *Journal of Geophysical Research*, *115*, F03028. https://doi.org/10.1029/2008JF001187

Haviv, I., Enzel, Y., Whipple, K. X., Zilberman, E., Stone, J., Matmon, A., & Fifield, L. K. (2006). Amplified erosion above waterfalls and oversteepened bedrock reaches. *Journal of Geophysical Research*, *111*, F04004. https://doi.org/10.1029/2006JF000461

Hayakawa, Y. S., & Matsukura, Y. (2003). Recession rates of waterfalls in Boso Peninsula, Japan, and a predictive equation. *Earth Surface Processes and Landforms*, *28*(6), 675–684. https://doi.org/10.1002/esp.519

Hayakawa, Y. S., & Matsukura, Y. (2010). Stability analysis of waterfall cliff face at Niagara Falls: An implication to erosional mechanism of waterfall. *Engineering Geology*, *116*(1–2), 178–183. https://doi.org/10.1016/j.enggeo.2010.08.004

Hayakawa, Y. S., Yokoyama, S., & Matsukura, Y. (2008). Erosion rates of waterfalls in post-volcanic fluvial systems around Aso volcano, southwestern Japan. *Earth Surface Processes and Landforms*, *33*(5), 801–812. https://doi.org/10.1002/esp.1615

Holland, W. N., & Pickup, G. (1976). Flume study of knickpoint development in stratified sediment. *Geological Society of America Bulletin*, *87*(1), 76–82. https://doi.org/10.1130/0016-7606(1976)87%3C76:fsokdi%3E2.0.co;2

Howard, A. D., Dietrich, W. E., & Seidl, M. A. (1994). Modeling fluvial erosion on regional to continental scales. *Journal of Geophysical Research*, *99*(B7), 13,971–13,986. https://doi.org/10.1029/94JB00744

Howard, A. D., & Kerby, G. (1983). Channel changes in badlands. *Geological Society of America Bulletin*, *94*(6), 739–752.

Izumi, N., Yokokawa, M., & Parker, G. (2017). Incisional cyclic steps of permanent form in mixed bedrock-alluvial rivers. *Journal of Geophysical Research: Earth Surface*, *122*, 130–152. https://doi.org/10.1002/2016JF003847

Johnson, J. P., Whipple, K. X., & Sklar, L. S. (2010). Contrasting bedrock incision rates from snowmelt and flash floods in the Henry Mountains, Utah. *Geological Society of America Bulletin*, *122*(9–10), 1600–1615. https://doi.org/10.1130/b30126.1

Joseph, G. G., Zenit, R., Hunt, M. L., & Rosenwinkel, A. M. (2001). Particle-wall collisions in a viscous fluid. *Journal of Fluid Mechanics*, *433*, 329–346.

Lague, D. (2014). The stream power river incision model: Evidence, theory and beyond. *Earth Surface Processes and Landforms*, *39*(1), 38–61. https://doi.org/10.1002/esp.3462

Lague, D., Hovius, N., & Davy, P. (2005). Discharge, discharge variability, and the bedrock channel profile. *Journal of Geophysical Research*, *110*, F04006. https://doi.org/10.1029/2004JF000259

Lamb, M. P., & Dietrich, W. E. (2009). The persistence of waterfalls in fractured rock. *Geological Society of America Bulletin*, *121*(7–8), 1123–1134. https://doi.org/10.1130/b26482.1

Lamb, M. P., Dietrich, W. E., & Sklar, L. S. (2008). A model for fluvial bedrock incision by impacting suspended and bed load sediment. *Journal of Geophysical Research*, *113*, F03025. https://doi.org/10.1029/2007JF000915

Lamb, M. P., Finnegan, N. J., Scheingross, J. S., & Sklar, L. S. (2015). New insights into the mechanics of fluvial bedrock erosion through flume experiments and theory. *Geomorphology*, *244*, 33–55. https://doi.org/10.1016/j.geomorph.2015.03.003

Lamb, M. P., Howard, A. D., Dietrich, W. E., & Perron, J. T. (2007). Formation of amphitheater-headed valleys by waterfall erosion after large-scale slumping on Hawai'i. *Geological Society of America Bulletin*, *119*(7–8), 805–822. https://doi.org/10.1130/b25986.1

Lapotre, M. G. A., Lamb, M. P., & Williams, R. M. E. (2016). Canyon formation constraints on the discharge of catastrophic outburst floods of Earth and Mars. *Journal of Geophysical Research: Earth Surface*, *121*, 1232–1263. https://doi.org/10.1002/2016JE005061

Launder, B. E., & Rodi, W. (1983). The turbulent wall jet – Measurements and modeling. *Annual Review of Fluid Mechanics*, *15*, 429–459.
Leopold, L. B., Wolman, M. G., & Miller, J. P. (1964). *Fluvial Processes in Geomorphology*. San Francisco, CA: W.H. Freeman.
Loget, N., & Van Den Driessche, J. (2009). Wave train model for knickpoint migration. *Geomorphology*, *106*(3–4), 376–382. https://doi.org/10.1016/j.geomorph.2008.10.017
Mackey, B. H., Scheingross, J. S., Lamb, M. P., & Farley, K. A. (2014). Knickpoint formation, rapid propagation, and landscape response following coastal cliff retreat at the last interglacial sea-level highstand: Kaua'i, Hawai'i. *Geological Society of America Bulletin*, *126*(7–8), 925–942. https://doi.org/10.1130/b30930.1
McLean, S. R. (1992). On the calculation of suspended-load for noncohesive sediments. *Journal of Geophysical Research*, *97*(C4), 5759–5770. https://doi.org/10.1029/91JC02933
Pagliara, S., Hager, W. H., & Minor, H. E. (2006). Hydraulics of plane plunge pool scour. *Journal of Hydraulic Engineering-Asce*, *132*(5), 450–461. https://doi.org/10.1061/(asce)0733-9429(2006)132:5(450)
Portenga, E. W., & Bierman, P. R. (2011). Understanding Earth's eroding surface with 10-Be. *GSA Today*, *21*(8), 4–10. https://doi.org/10.1130/G111A.1
Rajaratnam, N. (1976). *Turbulent Jets*. Amsterdam: Elsevier.
Roberts, G. G., & White, N. (2010). Estimating uplift rate histories from river profiles using African examples. *Journal of Geophysical Research*, *115*, B02406. https://doi.org/10.1029/2009JB006692
Robinson, K. M., Hanson, G. J., Cook, K. R., & Kadavy, K. C. (2001). Erosion of fractured materials. *Transactions of the Asae*, *44*(4), 819–823.
Rosenbloom, N. A., & Anderson, R. S. (1994). Hillslope and channel evolution in a marine terraced landscape, Santa-Cruz, California. *Journal of Geophysical Research*, *99*(B7), 14,013–14,029. https://doi.org/10.1029/94JB00048
Rouse, H. R. (1936). Discharge characteristics of the free overfall. *Civil Engineering*, *6*, 257–260.
Rouse, H. R. (1937a). Modern conceptions of the mechanics of turbulence. *Transactions of the American Society of Civil Engineers*, *102*(1), 463–543.
Rouse, H. R. (1937b). Pressure distribution and acceleration at the free overfall. *Civil Engineering*, *7*, 518.
Scheingross, J. S. (2016). *Mechanis of Sediment Transport and Bedrock Erosion in Steep Landscapes*. Pasadena, CA: California Institute of Technology.
Scheingross, J. S., Brun, F., Lo, D. Y., Omerdin, K., & Lamb, M. P. (2014). Experimental evidence for fluvial bedrock incision by suspended and bedload sediment. *Geology*, *42*(6), 523–526. https://doi.org/10.1130/G35432.1
Scheingross, J. S., & Lamb, M. P. (2016). Sediment transport through self-adjusting, bedrock-walled waterfall plunge pools. *Journal of Geophysical Research: Earth Surface*, *121*, 939–963. https://doi.org/10.1002/2015JF003620
Scheingross, J. S., Lo, D. Y., & Lamb, M. P. (2017). Self-formed waterfall plunge pools in homogeneous rock. *Geophysical Research Letters*, *44*, 200–208. https://doi.org/10.1002/2016GL071730
Schmeeckle, M. W., Nelson, J. M., Pitlick, J., & Bennett, J. P. (2001). Interparticle collision of natural sediment grains in water. *Water Resources Research*, *37*(9), 2377–2391. https://doi.org/10.1029/2001WR000531
Seidl, M. A., Dietrich, W. E., & Kirchner, J. W. (1994). Longitudinal profile development into bedrock – An analysis of Hawaiian channels. *Journal of Geology*, *102*(4), 457–474.
Sklar, L. S., & Dietrich, W. E. (2001). Sediment and rock strength controls on river incision into bedrock. *Geology*, *29*(12), 1087–1090. https://doi.org/10.1130/0091-7613(2001)029%3C1087:sarsco%3E2.0.co;2
Sklar, L. S., & Dietrich, W. E. (2004). A mechanistic model for river incision into bedrock by saltating bed load. *Water Resources Research*, *40*, W06301. https://doi.org/10.1029/2003WR002496
Stein, O. R., Alonso, C. V., & Julien, P. Y. (1993). Mechanics of jet scour downstream of a headcut. *Journal of Hydraulic Research*, *31*(6), 723–738. https://doi.org/10.1080/00221689309498814
Stein, O. R., & Julien, P. Y. (1993). Criterion delineating the mode of headcut migration. *Journal of Hydraulic Engineering ASCE*, *119*(1), 37–50. https://doi.org/10.1061/(asce)0733-9429(1993)119:1(37)
Stein, O. R., & LaTray, D. A. (2002). Experiments and modeling of head cut migration in stratified soils. *Water Resources Research*, *38*(12), 1284. https://doi.org/10.1029/2001WR001166
Stock, J. D., & Montgomery, D. R. (1999). Geologic constraints on bedrock river incision using the stream power law. *Journal of Geophysical Research*, *104*(B3), 4983–4993. https://doi.org/10.1029/98JB02139
Timoshenko, S. P., & Gere, J. M. (1978). *Mechanics of Materials* (pp. 552). New York: Van Nostrand Reinhold Co.
Valle, B. L., & Pasternack, G. B. (2006). Air concentrations of submerged and unsubmerged hydraulic jumps in a bedrock step-pool channel. *Journal of Geophysical Research*, *111*, F03016. https://doi.org/10.1029/2004JF000140
Verhoff, A. (1963). The two-dimensional, turbulent wall jet with and without an external free stream (Rep. 626). Princeton, NJ: Princeton University.
Weissel, J. K., & Seidl, M. A. (1997). Influence of rock strength properties on escarpment retreat across passive continental margins. *Geology*, *25*(7), 631–634. https://doi.org/10.1130/0091-7613(1997)025%3C0631:iorspo%3E2.3.co;2
Whipple, K. X., & Tucker, G. E. (1999). Dynamics of the stream-power river incision model: Implications for height limits of mountain ranges, landscape response timescales, and research needs. *Journal of Geophysical Research*, *104*(B8), 17,661–17,674. https://doi.org/10.1029/1999JB900120
Whipple, K. X., & Tucker, G. E. (2002). Implications of sediment-flux-dependent river incision models for landscape evolution. *Journal of Geophysical Research*, *107*(B2), 2039. https://doi.org/10.1029/2000JB000044
Whittaker, A. C. (2012). How do landscapes record tectonics and climate? *Lithosphere*, *4*(2), 160–164. https://doi.org/10.1130/Rf.L003.1
Wobus, C. W., Crosby, B. T., & Whipple, K. X. (2006). Hanging valleys in fluvial systems: Controls on occurrence and implications for landscape evolution. *Journal of Geophysical Research*, *111*, F02017. https://doi.org/10.1029/2005JF000406
Wobus, C. W., Tucker, G. E., & Anderson, R. S. (2010). Does climate change create distinctive patterns of landscape incision? *Journal of Geophysical Research*, *115*, F04008. https://doi.org/10.1029/2009JF001562
Yokokawa, M., Kotera, A., & Kyogoku, A. (2013). Cyclic steps by bedrock incision. In S. Fukuoka et al. (Eds.), *Advances in River Sediment Research* (pp. 629–633). The Netherlands: CRC Press.
Young, R. (1985). Waterfalls: Form and process. *Zeitschrift für Geomorphologie*, *55*, (Supplementband), 81–95.